International Journal of General Medicine

Dovepress
Taylor & Francis Group

Open Access Full Text Article

ORIGINAL RESEARCH

Evolocumab Alters Transcriptomic Signatures and Identifies Inflammatory Biomarkers in Brain-Heart Syndrome with Coronary Heart Disease History

Huijie Dong[1], Xing Gong[2], Zhenrong Zhao[1], Yuki Joyama[3], Xiaofei Ji[2,*], Peng Qu[4,*]

[1]Department of Cardiology, Second Affiliated Hospital of Dalian Medical University, Dalian, Liaoning, People's Republic of China; [2]Department of Neurology, First Affiliated Hospital of Dalian Medical University, Dalian, Liaoning, People's Republic of China; [3]Department of Gastroenterology and Hepatology, Tokyo Medical University, Tokyo, Japan; [4]Institute of Heart and Vessel Diseases, Second Affiliated Hospital of Dalian Medical University, Dalian, Liaoning, People's Republic of China

*These authors contributed equally to this work

Correspondence: Peng Qu, Institute of Heart and Vessel Diseases, Second Affiliated Hospital of Dalian Medical University, Dalian, Liaoning, People's Republic of China, Email qupeng777@aliyun.com; Xiaofei Ji, Department of Neurology, First Affiliated Hospital of Dalian Medical University, Dalian, Liaoning, People's Republic of China, Email jixiaofei1979@163.com

Purpose: A history of coronary heart disease (CHD) increases the risk of Brain-Heart Syndrome (BHS) after acute stroke, partly through heightened inflammatory responses. Evolocumab, a PCSK9 inhibitor, has anti-inflammatory properties, but its transcriptomic effects in BHS patients with CHD remain unclear. This study aims to identify evolocumab-associated transcriptomic changes and inflammation-related biomarkers in this population.

Patients and Methods: Blood samples from 24 BHS patients with CHD history (12 receiving rosuvastatin alone, 12 receiving rosuvastatin plus evolocumab) underwent transcriptomic sequencing. Candidate biomarkers were identified via differential expression and machine learning, with functional enrichment and immune infiltration analyses conducted.

Results: Four candidate biomarkers were identified: *WHRN (DFNB31)*, *IL12A*, and *ASB14* were upregulated, while *TMED7-TICAM2* was downregulated in the evolocumab combination group. These genes were enriched in pathways related to cell metabolism, signal transduction, and immune regulation. Immune infiltration analysis showed modest but detectable changes in B-cell subsets. External validation confirmed differential expression of these candidate biomarkers in CAD patients.

Conclusion: This pilot study provides preliminary insights into the molecular mechanisms of evolocumab in treating Brain-Heart Syndrome with a coronary heart disease history, identifying four inflammation-related biomarkers. These findings suggest potential targets for future investigation; however, given the exploratory nature and small sample size, further experimental and clinical validation is required before any therapeutic application.

Keywords: evolocumab, coronary heart disease, brain-heart syndrome, transcriptomics

Introduction

Brain-Heart Syndrome (BHS) is a clinical syndrome developed due to cardiac insufficiency or myocardial dysfunction caused by severe central nervous system diseases. It has a high incidence and mortality rate, seriously affects the prognosis of stroke, and is the second leading cause of death in cerebrovascular diseases.[1] A history of coronary heart disease (CHD) is a major risk factor for BHS.[2]

Elevated low-density lipoprotein cholesterol (LDL-C), a common risk factor for both conditions, drives atherosclerosis, causing vascular stenosis and hypoperfusion. Oxidized low - density lipoprotein (ox - LDL) further exacerbates vascular damage by triggering pro - inflammatory pathways. This common pathophysiological mechanism not only affects the cerebral blood vessels but also the coronary arteries, forming the common pathological basis of BHS.[3] In acute ischemic stroke (AIS) patients with CHD, intracranial/extracranial, anterior-posterior circulation involvement, and ≥50% head and neck artery

https://doi.org/10.2147/IJGM.S603395
Received: 13 February 2026
Accepted: 17 May 2026
Published: 22 May 2026

Graphical Abstract

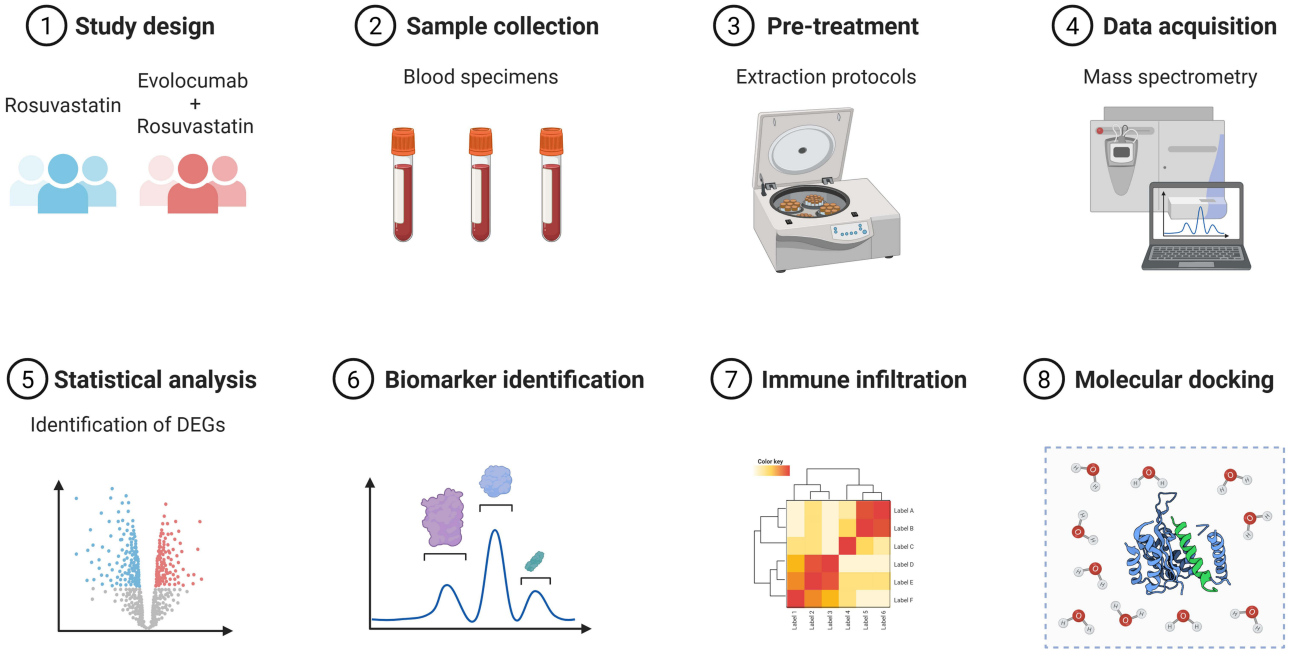

stenosis are more prevalent.[4] BHS patients with CHD exhibit early innate immune memory and immune training, increasing pro-inflammatory cytokine production. Macrophages, key innate immune cells, recognize Ox-LDL and lipoproteins (a) [Lp (a)] through scavenger receptors (SRs) and toll-like receptors (TLRs), inducing innate immune memory.[5–8] Initial stimulation with Ox-LDL and Lp (a) primes monocytes to become macrophages, which upon subsequent TLR2/4 activation, overproduce TNF-α and IL-6, further destabilizing plaques.

Proprotein convertase subtilisin/kexin type 9 (PCSK9) is a key regulatory factor in vascular inflammation. In atherosclerotic diseases, excessive PCSK9 reduces LDL-C receptor expression and uptake, promotes LDL-C retention in the vascular wall, and generates more ox-LDL,[9] Mononuclear macrophages enriched with ox-LDL promote inflammatory responses by upregulating proinflammatory cytokines and chemokines (such as IL-1β, IL-6, TNF-α, CCR-2, and M-CSF-1),[10] exacerbating vascular wall damage. Moreover, PCSK9 can activate the TLR4/NF-κB signaling pathway independently of lipid metabolism, significantly aggravating vascular inflammatory responses.[11] This mechanism operates in both cardiovascular and cerebrovascular systems, providing a common inflammatory basis for CHD and BHS.

Evolocumab, a PCSK9 inhibitor, has rapid onset and potent lipid-lowering effects. The FOURIER study showed that long-term evolocumab use reduces LDL-C by 59% and significantly lowers primary endpoint events in patients with a history of non-hemorrhagic cerebrovascular disease.[12] PCSK9 inhibitors also reduce microglial activation in BHS and alleviate central neuroimmune injury.[13] Previous studies indicate that nontraumatic intracranial hemorrhage can trigger sudden death through acute neurovascular injury, supporting the concept of brain–heart interaction and subsequent systemic inflammatory and cardiovascular dysregulation.[14] Although our preliminary studies have found that evolocumab in acute ischemic stroke reduces peripheral IL-6 elevation,[15] controversy remains over whether PCSK9 inhibitors have direct anti-inflammatory effects independent of lipid-lowering, as their impact on systemic inflammatory markers like hs-CRP is limited.[16]

Despite this controversy, the significant cardiovascular benefits of PCSK9 inhibitors suggest additional mechanisms beyond lipid-lowering. We hypothesize that evolocumab, on top of its lipid-lowering effects, may modulate transcriptomic signatures associated with inflammatory pathways and immune cell function in BHS patients with a history of CHD. However, the transcriptomic mechanisms of evolocumab in this population remain poorly understood. Therefore,

this study aims to explore, through transcriptome analysis of peripheral blood samples, the key gene expression changes regulated by evolocumab in BHS patients with CHD history, thereby investigating its possible regulatory mechanism on the acute-phase inflammatory response.

Material and Methods

Data Collection

This study collected blood samples from 12 BHS patients with CHD history who were treated with rosuvastatin (rosuvastatin-only group) and 12 BHS patients with CHD history treated with rosuvastatin combined with evolocumab at the First Affiliated Hospital of Dalian Medical University for transcriptome sequencing. All participants provided signed consent forms, and the study was approved by the Ethics Committee of the First Affiliated Hospital of Dalian Medical University (Approval number: PJ-KS-KY-2025-958).

External validation independent datasets were obtained from the Gene Expression Omnibus (GEO, https://www.ncbi.nlm.nih.gov/geo/). GSE113079 (GPL20112) was selected as the primary validation dataset, which includes 93 CAD patients and 48 healthy controls, representing the largest available sample size for CAD-related validation. The single-cell RNA sequencing dataset GSE121893 (GPL18573) was also retrieved from GEO for cellular-level analysis.

Transcriptomic

Sequencing and Data Preprocessing. Total RNA was isolated from 24 blood specimens and purified using TRIzol reagent (ThermoFisher, 15596018, California, USA). RNA was then quantified and its purity was checked using Thermo Fisher Qubit 3.0 (ThermoFisher, Q33216, California, USA) and Agilent 5300 Fragment Analyzer (Agilent, CA, USA, M5311AA). High-quality RNA samples with an RIN exceeding 7.0 were selected for sequencing library construction. Subsequently, mRNA was purified using mRNA Capture Beads 2.0 (Yeasen Cat.12629ES, China) and fragmented with magnesium ions (Yeasen Cat.12340ES97, CHN) at 94°C. First-strand cDNA was synthesized using reverse transcriptase, and second-strand DNA was generated using E. coli DNA polymerase I, RNase H, and dUTP Solution (Yeasen Cat.12340ES97, CHN). After end-repair and adapter ligation, PCR amplification was performed (Supplementary Table 1), resulting in a cDNA library with an average insert size of 400±50 bp. The library was sequenced on the Illumina Novaseq™ X Plus platform (LC-Bio Technology CO., Ltd., Hangzhou, China) with 2×150 bp paired-end sequencing. Raw sequencing data was processed with Cutadapt (https://cutadapt.readthedocs.io/en/stable/, v 1.9) to remove low-quality reads and adapter contamination. Sequence quality was confirmed with FastQC (https://www.bioinformatics.babraham.ac.uk/projects/fastqc/, v 0.11.9), generating high-quality clean reads. These clean reads were then mapped to the reference genome (Homo sapiens, GRCh38) using HISAT2 (https://daehwankimlab.github.io/hisat2/, v 2–2.2.1). Gene expression levels were quantified by calculating the FPKM value [FPKM = total exon fragments/mapped reads (millions) × exon length (kb)] using StringTie (https://ccb.jhu.edu/software/stringtie/, v 2.1.6) and ballgown (https://www.bioconductor.org/packages/release/bioc/html/ballgown.html). Boxplots were drawn with the "ggplot2" package (v 3.5.1)[17] for visualization, providing a basis for subsequent transcriptomics data analysis.

Acquisition of Candidate Genes and Functional Enrichment Analysis

To obtain candidate genes in the rosuvastatin-only and evolocumab plus rosuvastatin groups, differential expression analysis was performed using the "DESeq2" package (v 1.38.0)[18] default Wald test with the criteria of |log2 fold change (FC)|>1.0 and p.adj<0.05. Genes with low expression were filtered using the criterion that a gene must have a count ≥2 in at least 3 samples. The resulting genes were defined as candidate genes. Then, to visually present the distribution of these genes, a volcano plot was created using the "ggplot2" package (v 3.5.1). In addition, to further illustrate the expression levels of these genes, a heatmap of the expression of the top 10 upregulated and top 10 downregulated genes, selected based on the highest |log2FC|, was plotted using the "pheatmap" package (v 1.0.12).[19] Subsequently, to explore the biological functions and signaling pathways involved by the candidate genes, Gene Ontology (GO) annotation analysis (including Biological Process (BP), Cellular Components (CC), and Molecular Functions (MF)) and Kyoto Encyclopedia of Genes and Genomes (KEGG) pathway enrichment analysis ($p < 0.05$) were carried out using the "clusterProfiler"

package (v 4.8.3).[20] For functional enrichment analysis, we applied the Benjamini-Hochberg method for multiple testing correction and set the significance threshold at adjusted p-values (p.adj) < 0.05 to identify significantly enriched pathways. The results were visualized using "ggplot2" (v 3.5.1) and "Enrichplot" packages (v 1.18.4).[21] Finally, to investigate the protein-level interactions of candidate genes, a protein-protein interaction (PPI) network was constructed using the Search Tool for the Retrieval of Interacting Genes/Proteins (STRING) database (https://string-db.org) (confidence > 0.4), and the network was visualized using Cytoscape software (v3.10.3).[22]

Machine Learning and Identification of Candidate Biomarkers

To further screen candidate biomarkers, three machine learning methods were employed. First, using the "glmnet" package (v 4.1–4)[23] on all transcriptome data, a least absolute shrinkage and selection operator (LASSO) regression model was built for candidate genes using the minimum lambda value and non-zero coefficients (5-fold cross-validation). Meanwhile, the "e1071" package (v 1.7.14)[24] was used to analyze candidate genes with the support vector machine-recursive feature elimination (SVM-RFE) algorithm according to 5-fold cross-validation. Boruta analysis was performed using the "Boruta" package (v 8.0.0)[25] with parameters pValue = 0.05, mcAdj = TRUE, and maxRuns = 500. Feature importance was evaluated using random forest, and features were classified as "confirmed", "tentative", or "rejected" based on their importance scores relative to shadow features. To mitigate the risk of overfitting associated with the small sample size (n=24), we combined the three machine learning algorithms via "ggVennDiagram" package (v 1.2.2)[26] and took the intersection of their selected features to identify candidate biomarkers. Based on all transcriptome sample data, the "pROC" package (v 1.18.0)[27] was used to plot receiver operating characteristic (ROC) curves for candidate biomarkers and determine the area under the curve (AUC). Biomarkers with an AUC>0.7 were regarded as candidate biomarkers. Finally, the Wilcoxon test was applied to compare the expression differences of these candidates between the rosuvastatin-only and evolocumab plus rosuvastatin groups in the transcriptomic data ($p<0.05$), and boxplots were created using the "ggplot2" package (v 3.5.1). To validate the generalizability of the identified candidate biomarkers, we performed external validation using an independent dataset. The Wilcoxon rank-sum test was used to assess expression differences between control groups, with statistical significance set at $p < 0.05$. To evaluate the diagnostic performance of these candidate biomarkers, we constructed receiver operating characteristic (ROC) curves and calculated the area under the curve (AUC) values using the "pROC" package (v 1.18.0).[27]

GeneMANIA and Gene Set Enrichment Analysis (GSEA) Analyses

To uncover other genes and biological functions related to the candidate biomarkers' functions, a co-expression network was established via the GeneMANIA database (https://www.genemania.org/). Then, to further explore the signaling pathways and potential biological functions implicated by the candidate biomarkers, GSEA was performed. Using the "c2.cp.kegg.v7.4.symbols.gmt" gene set from the Molecular Signatures Database (MSigDB) (https://www.gsea-msigdb.org/gsea/msigdb) as the background, Spearman correlation analysis between each candidate biomarker and other genes was carried out using the "psych" package (v 2.2.9)[28] with the criteria of |correlation coefficients (cor)| > 0.3 and $p < 0.05$. Based on the correlation coefficients ranked from largest to smallest, GSEA pathway enrichment analysis was performed using the "clusterProfiler" package with the criteria of |normalized enrichment score (NES)|>1, false discovery rate (FDR)<0.25, and Benjamini-Hochberg adjusted p-value<0.05.

Immune Infiltration Analysis

To comprehensively elucidate the immunophenotypic profiles of immune cells during evolocumab treatment in patients with BHS complicated by CHD, systematic immune infiltration analysis was performed across all study samples using the CIBERSORT algorithm. CIBERSORT is a computational method widely applied in tumor immunology research that uses linear regression models trained on known immune cell gene expression profiles to estimate relative abundances of immune cell subsets in mixed cell samples. This algorithm was employed to compare immune infiltration differences among 22 immune cell types based on the LM22 gene signature matrix ($p < 0.05$). Stacked plots displaying the abundance proportions of 22 immune cell types in each sample were generated using the "ggplot2" R package (v 3.5.1).[29] The non-parametric Wilcoxon rank-sum test was applied to identify significant differences in immune cell

infiltration between the rosuvastatin-only and evolocumab plus rosuvastatin treatment groups, with statistical significance set at $p < 0.05$ to screen for differentially infiltrated immune cell populations. Box plots were generated using the "ggplot2" R package (v 3.5.1)[29] for graphical representation of immune cell proportions between treatment groups. Finally, Spearman correlation analysis was performed using the "psych" R package (v 2.2.9)[30] to explore interrelationships among differentially infiltrated immune cell types and associations between these immune cells and relevant candidate biomarkers. Additionally, Mantel test correlation analysis was conducted between key genes and immune cells, with analyses having correlation coefficients ($|cor| > 0.30$ and $p < 0.05$ considered statistically significant.

Single-Cell RNA Sequencing Data Preprocessing, Cell Annotation, and Functional Analysis

To investigate cellular-level gene expression patterns in CAD, we analyzed single-cell RNA sequencing data. We constructed a Seurat object using the "CreateSeuratObject" function from the R package "Seurat" (v 5.0.1),[31] initially containing 2,152 cells and 21,543 genes. Quality control was performed to retain high-quality cells using the following criteria: 200 < nFeatures < 6000 and 200 < nCount_RNA < 30000, resulting in 1,630 high-quality cells. Data normalization was performed using the "NormalizeData" function, followed by identification of 2,000 highly variable genes using the "FindVariableFeatures" function. The top 10 genes with the highest standard deviation were annotated. Principal component analysis (PCA) was conducted using the "RunPCA" function on highly variable genes, and the optimal number of principal components was determined using the "ElbowPlot" function. Based on signal stabilization patterns, the first 16 principal components were selected for subsequent clustering analysis ($p < 0.05$). Cell clustering was performed using the "FindClusters" function with a resolution parameter of 0.9. Uniform Manifold Approximation and Projection (UMAP) was applied for dimensionality reduction and visualization of different cell clusters. Marker genes for each cluster were identified using the "FindAllMarkers" function with thresholds: logfc.threshold = 0.5, min.pct = 0.25, and only.pos = TRUE. Cell clusters were annotated based on marker genes from literature[32] and the CellMarker database (https://xteam.xbio.top/CellMarker/). Marker gene expression patterns across different cell clusters were visualized using bubble plots. Functional enrichment analysis was performed on different cell clusters using the R package "ReactomeGSA" (v 1.12.0)[33] to explore biological pathways. The Reactome database, which records relationships between signaling and metabolic molecules and their constituent biological pathways and processes, was used to annotate biological pathways in different cell clusters. The top 10 enriched pathways were visualized using heatmaps. The distribution of candidate biomarkers within cells was displayed using UMAP. Cell proportions between CAD and control samples were compared using the "ggplot2" (v 3.3.6) package.[29] Cardiomyocytes showing differential expression of key genes between CAD and control samples were defined as key cells using the Wilcoxon rank-sum test ($p < 0.05$).

Cell Communication and Pseudotime Trajectory Analysis

Cell-cell communication analysis was performed using CellChat, a computational tool for studying ligand-receptor interactions. CellChat was used to analyze the maximum number of interactions and interaction weights for each cell in the single-cell dataset, infer communication probabilities at the signaling pathway level, and construct ligand-receptor networks. The quantity and intensity of cellular interactions between key cells and other cell types were visualized through communication networks. Ligand-receptor pairs and receptor-ligand pairs between key cell types and other cell types were displayed using bubble plots ($p < 0.05$).

To understand the differentiation trajectory of key cells, pseudotime trajectory analysis was performed using "Monocle2" (v 2.20.1).[34] Key cell types were first re-clustered into 3 subclusters through UMAP dimensionality reduction and clustering analysis. Pseudotime trajectory analysis was conducted using the "reduceDimension" function, and cells were ordered along trajectories based on temporal gene expression using the "orderCells" function. The analysis identified 5 differentiation states, with branches representing cell state transitions visualized using "plot_cell_trajectory". The expression patterns of candidate biomarkers across different differentiation stages were evaluated to reveal their changes along cell differentiation trajectories.

Inclusion and Exclusion Criteria for All Subjects

Inclusion Criteria

Age within the range of 18 to 80 years.

Diagnosis of cerebrocardiac syndrome within 24 hours of ischemic stroke onset.

1≤ National Institute of Health Stroke Scale ≤15.

The current ischemic stroke is diagnosed as large artery atherosclerotic stroke according to the TOAST (Trial of Org 10172 in Acute Stroke Treatment) classification.

The level of high-sensitivity cardiac Troponin I on the first day of onset is greater than 0.114ug/L.

Confirmed history of atherosclerotic coronary heart disease (stable angina pectoris, unstable angina pectoris and myocardial infarction).

Availability of complete clinical data, including demographic, laboratory, and treatment-related information.

Written informed consent was obtained from the patient or legal guardian.

Exclusion Criteria

History of hemorrhagic stroke, including subarachnoid hemorrhage and intracerebral hemorrhage.

Presence of cerebral arteriovenous malformations or intracranial neoplasms.

Severe comorbidities, including but not limited to:

Severe infections are defined by at least one of the following criteria: body temperature ≥ 38 °C, signs of septic shock, infection-induced altered mental status, or respiratory failure (arterial oxygen partial pressure [PO2] < 60 mmHg).

Abnormal liver function is indicated by elevated alanine aminotransferase (ALT > 100 U/L) or aspartate aminotransferase (AST > 80 U/L).

Impaired renal function, defined by an estimated glomerular filtration rate (eGFR) < 30 mL/min/1.73m^2.

Active autoimmune or immunodeficiency disorders.

PCSK9 inhibitors were used within three months before the index event.

Incomplete clinical data could potentially bias the study results.

Statistical Analysis

All statistical analyses were conducted using R statistical software (version 4.3.1). For the retrospective analysis of inflammatory factors, group differences were evaluated using the Wilcoxon rank-sum test, with statistical significance set at $p < 0.05$. Baseline characteristics were analyzed using appropriate statistical tests: Student's *t*-test or nonparametric tests (eg., Mann–Whitney *U*-test) for continuous variables, and chi-square tests or Fisher's exact tests for categorical variables.

Results

The Identification and Functional Enrichment of 36 Candidate Genes

Transcriptomic sequencing samples showed balanced overall expression, with no batch effects detected (Figure 1a), ensuring the data's reliability and validity. The 36 candidate genes were identified through differential expression analysis (evolocumab plus rosuvastatin vs rosuvastatin-only), including 12 up-regulated genes and 24 down-regulated genes in the evolocumab plus rosuvastatin group (Figure 1b), and expression heatmaps of the top 10 up-regulated and top 10 down-regulated candidate genes were presented (Figure 1c).

GO functional enrichment of the 36 candidate genes revealed six significantly enriched cellular component (CC) terms: specific granule, tertiary granule, tertiary granule membrane, specific granule membrane, primary lysosome, and azurophil granule (Figure 1d and Supplementary Table 2). No biological process (BP) or molecular function (MF) terms reached significance. Notably, these enriched granule and lysosome structures are involved in inflammatory mediator storage, immune cell degranulation, and signal transduction, supporting the biological relevance of these genes in evolocumab treatment. KEGG pathway enrichment analysis was conducted on the 36 candidate genes, resulting in 21 significantly enriched pathways ($p < 0.05$). The top ten pathways with the highest number of enriched genes were displayed, including: Inflammatory bowel disease, cAMP signaling pathway, Pertussis, Leishmaniasis, ErbB signaling

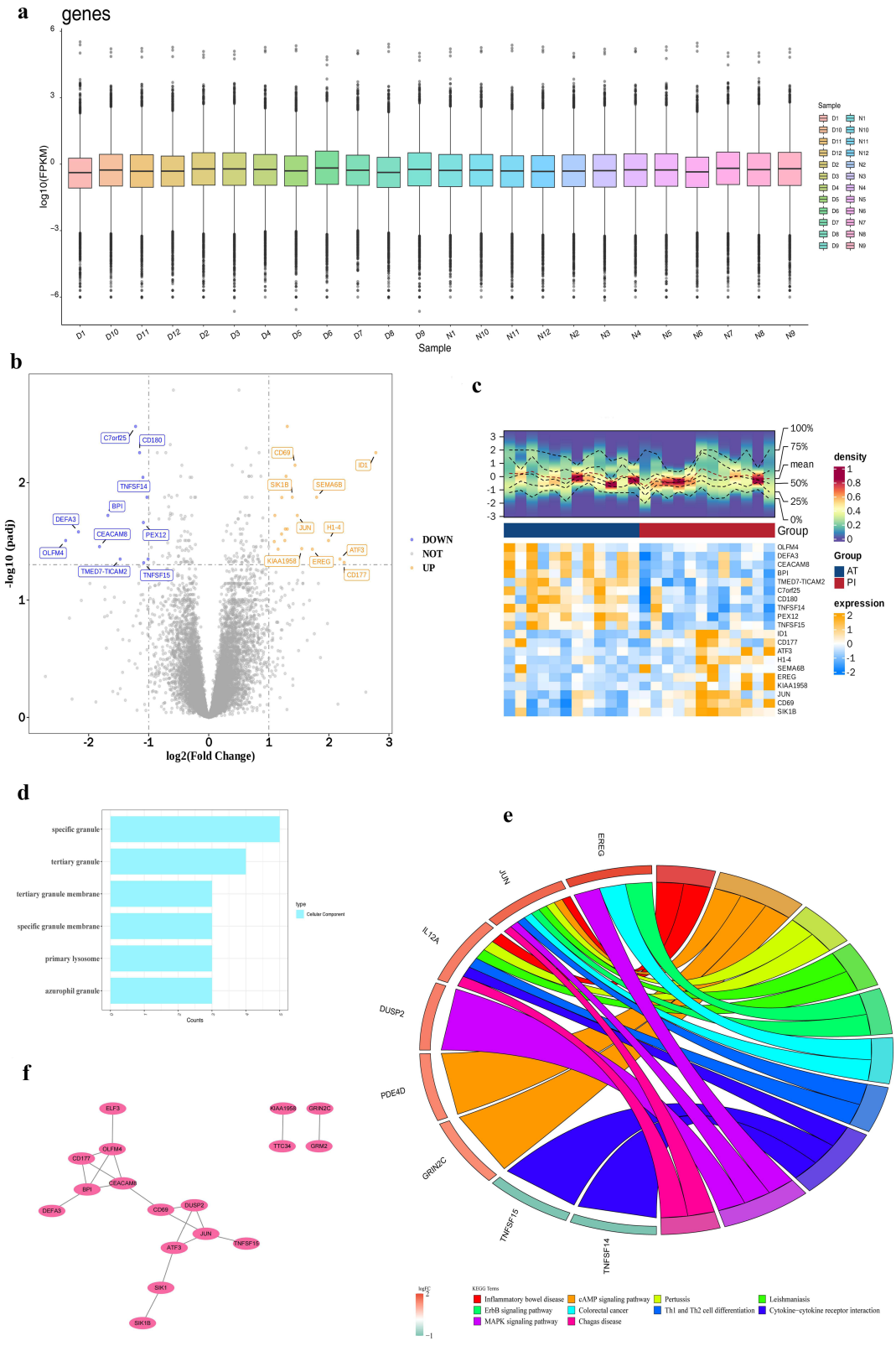

Figure 1 Identification of candidate functional genes. (**a**) Balanced detection of the expression of transcription samples; (**b**) Volcano plot of differential genes: The genes marked in the Figure are the top 10 up-regulated genes and the top 10 down-regulated genes with the largest |log2(FoldChange)|; (**c**) Heat map of differential gene expression; (**d**) GO enrichment analysis: The abscissa Counts represent the number of genes enriched, and the ordinate represents the names of BP, CC, and MF; (**e**) KEGG enrichment analysis: On the right side of the chord diagram are the top 10 KEGG pathways enriched, and on the left side are the genes corresponding to the pathways. The blue color of the gene module represents down-regulation; The internal lines represent the enrichment relationship between genes and KEGG pathways; (**f**) PPI network: Each node in the Figure represents a gene, each edge represents the protein-protein interaction of gene expression between genes, and the shade of color represents the connectivity of the nodes.

https://doi.org/10.2147/IJGM.S603395

pathway, Colorectal cancer, Th1 and Th2 cell differentiation, Chagas disease, Cytokine-cytokine receptor interaction, and MAPK signaling pathway (Figure 1e and Supplementary Table 3). These results indicated that the candidate genes could function critically in evolocumab-based treatment by regulating granule-related structures, lysosome functions, and signaling pathways involved in inflammation, immune cell differentiation, and cellular communication. Moreover, in the PPI network, CEACAM8 was found to interact with several candidate genes at the protein level, such as *BPI, OLFM4,* and *CD69* (Figure 1f), and these interactions might influence the mechanism or effectiveness of evolocumab-based treatment.

Identify and External Validation of Four Candidate Biomarkers

This study identified 8 LASSO feature genes (lambda.min=−2.2682): *WHRN (DFNB31), C7orf25, IL12A, ASB14, CLEC5A, SIK1B, DEFA3,* and *TMED7-TICAM2* (Figure 2a); 7 SVM-RFE feature genes: *WHRN, IL12A, ASB14, TNFSF14, PEX12, TMED7-TICAM2*, and *BPI* (Figure 2b); and 17 Boruta feature genes: *WHRN, C7orf25, ID1, TTC34, IL12A, TNFSF14, ASB14, CLEC5A, SIK1B, SAPCD1, BPI, ELF3, PEX12, PGAP1, CEACAM8, KIAA1958,* and *TMED7-TICAM2* (Figure 2c). By taking the intersection, the four genes *WHRN, IL12A, ASB14,* and *TMED7-TICAM2* were screened out as candidates (Figure 2d) and were ultimately identified as biomarkers (AUC>0.7) (Figure 2e). In the evolocumab plus rosuvastatin group, *WHRN, IL12A*, and *ASB14* expression levels were upregulated ($p<0.001$), while *TMED7-TICAM2* expression was significantly downregulated ($p<0.01$) (Figure 2f), providing a solid theoretical basis for studying evolocumab in treating BHS with CHD. External validation was performed across three independent datasets to assess biomarker generalizability. In the primary validation dataset GSE113079, expression analysis revealed that all four candidates showed significant differences between CAD patients and controls (Figure 2g). ROC analysis demonstrated AUC values of 0.647, 0.698, 0.659, and 0.668 for *WHRN, IL12A, ASB14*, and *TMED7-TICAM2*, respectively (Figure 2h), indicating that these candidate biomarkers have limited standalone diagnostic value and require further validation.

Revealing Functional Enrichment of Four Candidate Biomarkers

Through GeneMANIA, 20 genes related to the candidate biomarkers were identified, such as *WHRN, IL12A, ASB14,* and *TMED7-TICAM2*. These genes were found to form a co-expression network mainly through physical interactions, and likely interacted with other genes via co-expression, co-localization, and signaling pathways to perform biological functions (Figure 3a). These genes were primarily enriched in functions like positive regulation of leukocyte proliferation. GSEA results indicated that WHRN was enriched in KEGG pathways (Figure 3b and Supplementary Table 4), including SNARE interactions in vesicular transport, spliceosome, circadian rhythm-mammal, and ribosome; *IL12A* was enriched in KEGG pathways (Figure 3c and Table S4), with significant enrichment in cell cycle pathway; *ASB14* showed enrichment in ribosome pathway (Figure 3d and Table S4); and *TMED7-TICAM2* was enriched in multiple KEGG pathways (Figure 3e and Table S4), including proteasome, lysosome, Huntington's disease, citrate cycle (TCA cycle), and oxidative phosphorylation. Notably, ribosome pathway was commonly enriched across multiple candidate biomarkers (*WHRN, ASB14, and TMED7-TICAM2*), while spliceosome, SNARE interactions in vesicular transport, and circadian rhythm-mammal pathways were shared between *WHRN* and *TMED7-TICAM2* (adjusted $p < 0.05$). In the evolocumab intervention for BHS with CHD history, these candidate biomarkers were closely linked to processes like cellular metabolism, signal transduction, immune regulation, and cell cycle regulation.

Revealing the relationships between candidate biomarkers and differentially infiltrated immune cell types CIBERSORT analysis revealed distinct immune cell compositions between the rosuvastatin-only and evolocumab plus rosuvastatin groups across 22 immune cell subsets (Figure 4a). Both groups displayed multiple immune cell types, including B cells, dendritic cells, macrophages, mast cells, monocytes, neutrophils, NK cells, plasma cells, and various T cell subsets. Stacked plots illustrated the relative abundance distribution of each immune cell type across individual samples. Wilcoxon rank-sum test analysis of immune cell infiltration differences revealed that among the 22 immune cell types, only memory B cells and naive B cells showed significant differences between groups ($p < 0.05$) (Figure 4b). Memory B cells demonstrated significantly higher infiltration levels in the evolocumab plus rosuvastatin group compared to the rosuvastatin only group, while naive B cells exhibited the opposite trend. The remaining 20 immune cell types

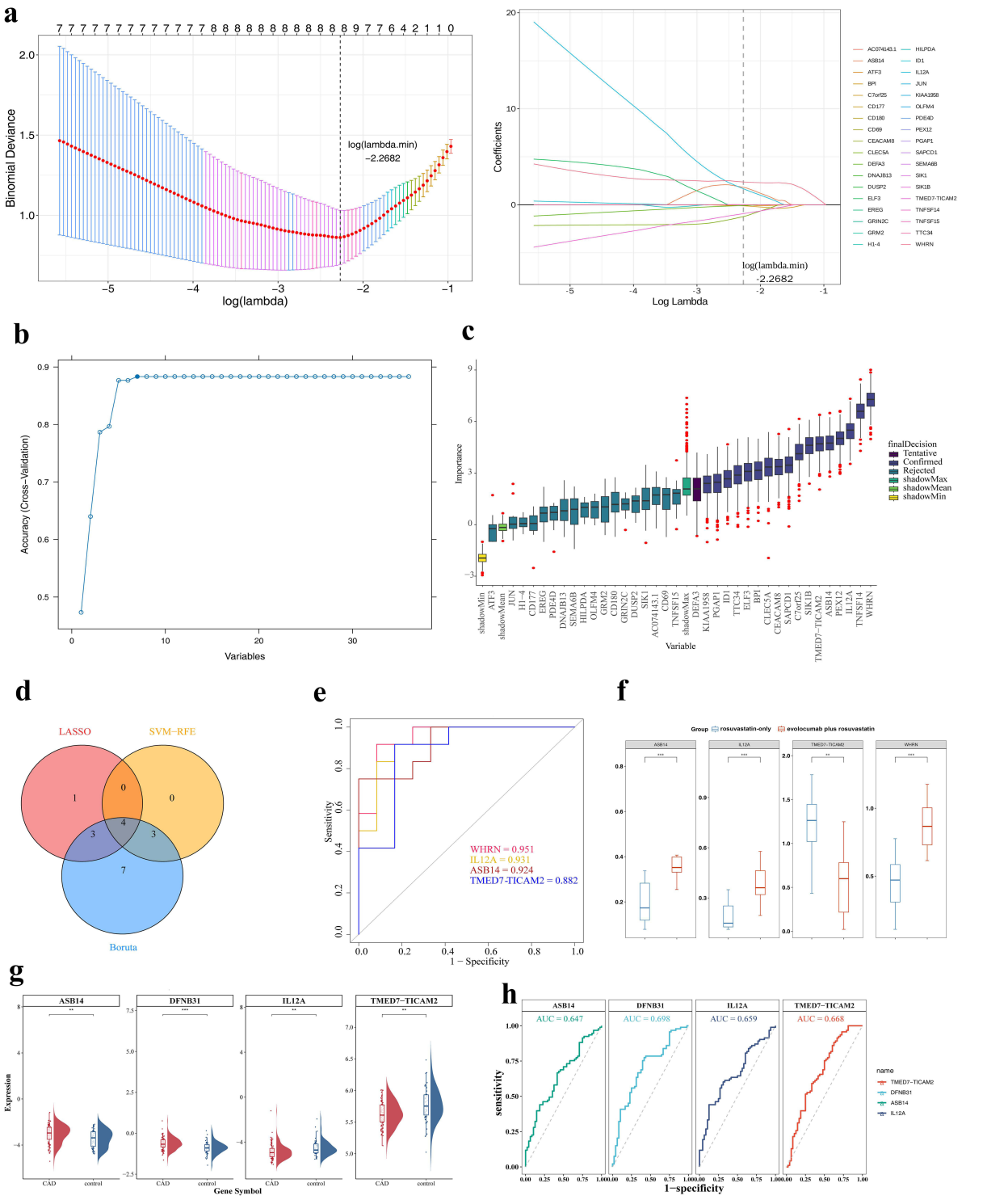

Figure 2 Identification and validation of biomarkers. (**a**) LASSO regression penalty coefficient plot (left) and 5-fold cross-validation plot for adjusting parameter selection in the LASSO algorithm (right); (**b**) SVM-RFE algorithm analysis: The abscissa represents the number of characteristic genes, and the ordinate represents the prediction accuracy of the SVM-RFE model. In the figure, when the number of genes is 7, the accuracy of the model is the highest, which is marked with a solid circle; (**c**) Boruta algorithm: The horizontal axis represents the characteristic genes, and the vertical axis represents the importance scores of the features. The final states are divided into three types: "Rejected", "Tentative", and "Confirmed"; (**d**) Intersection genes of the three algorithms: Red represents the LASSO algorithm, yellow represents the SVM-RFE algorithm, and blue represents the Boruta algorithm; (**e**) ROC curve: The abscissa, 1-Specificity (FPR) of the graph, represents the false positive rate, and the ordinate represents the sensitivity. An AUC > 0.7 indicates that the genes have a high predictive ability for the diagnosis of DR; (**f**) Analysis of the expression levels of key genes in different groups. (**g**) Expression levels of four biomarkers in the GSE113079 dataset. *ASB14, DFNB31, IL12A*, and *TMED7-TICAM2* showed differential expression between the CAD and control groups. (**h**) ROC curves of four biomarkers in the GSE113079 dataset. AUC values were 0.647, 0.698, 0.659, and 0.668 for *ASB14, DFNB31, IL12A,* and *TMED7-TICAM2*, respectively, reflecting their discriminatory ability for CAD. ** indicate $p < 0.01$, *** indicate $p < 0.001$.

https://doi.org/10.2147/IJGM.S603395

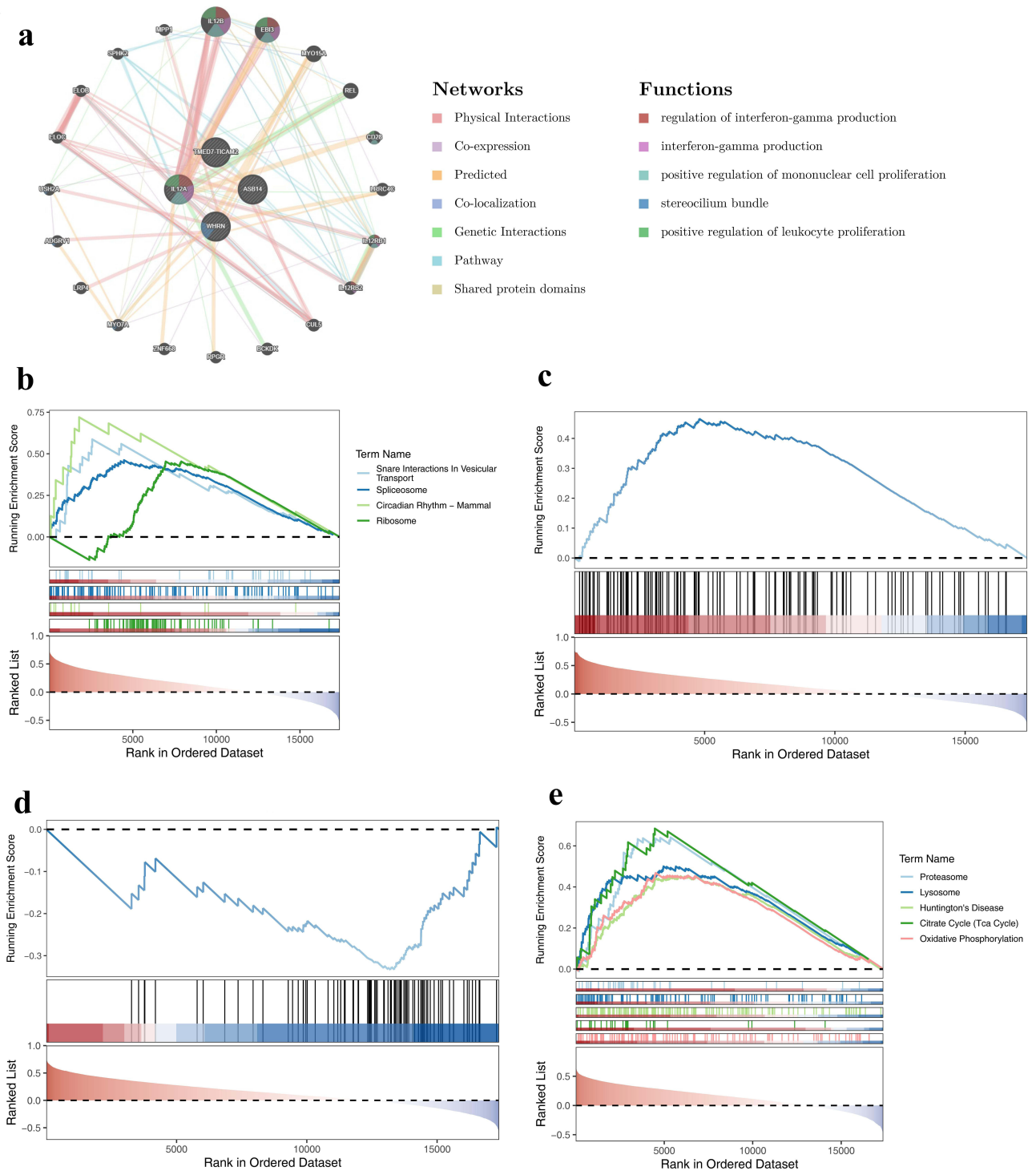

Figure 3 Functional enrichment of four biomarkers. (**a**) GeneMANIA analysis; (**b**) GSEA enrichment analysis of *WHRN*; (**c**) GSEA enrichment analysis of *IL12A*; (**d**) GSEA enrichment analysis of *ASB14*; (**e**) GSEA enrichment analysis of *TMED7-TICAM2*.

showed no significant differences between groups (ns, $p \geq 0.05$). Spearman correlation and Mantel test analyses revealed association patterns between the four candidate biomarkers (*WHRN, IL12A, ASB14, TMED7-TICAM2*) and the 22 immune cell types (Figure 4c). These results suggest that evolocumab treatment may have a limited but detectable impact on B-cell subsets; however, the absence of significant changes in most immune cell types indicates that the immunomodulatory effects of evolocumab are likely modest and should be interpreted with caution.

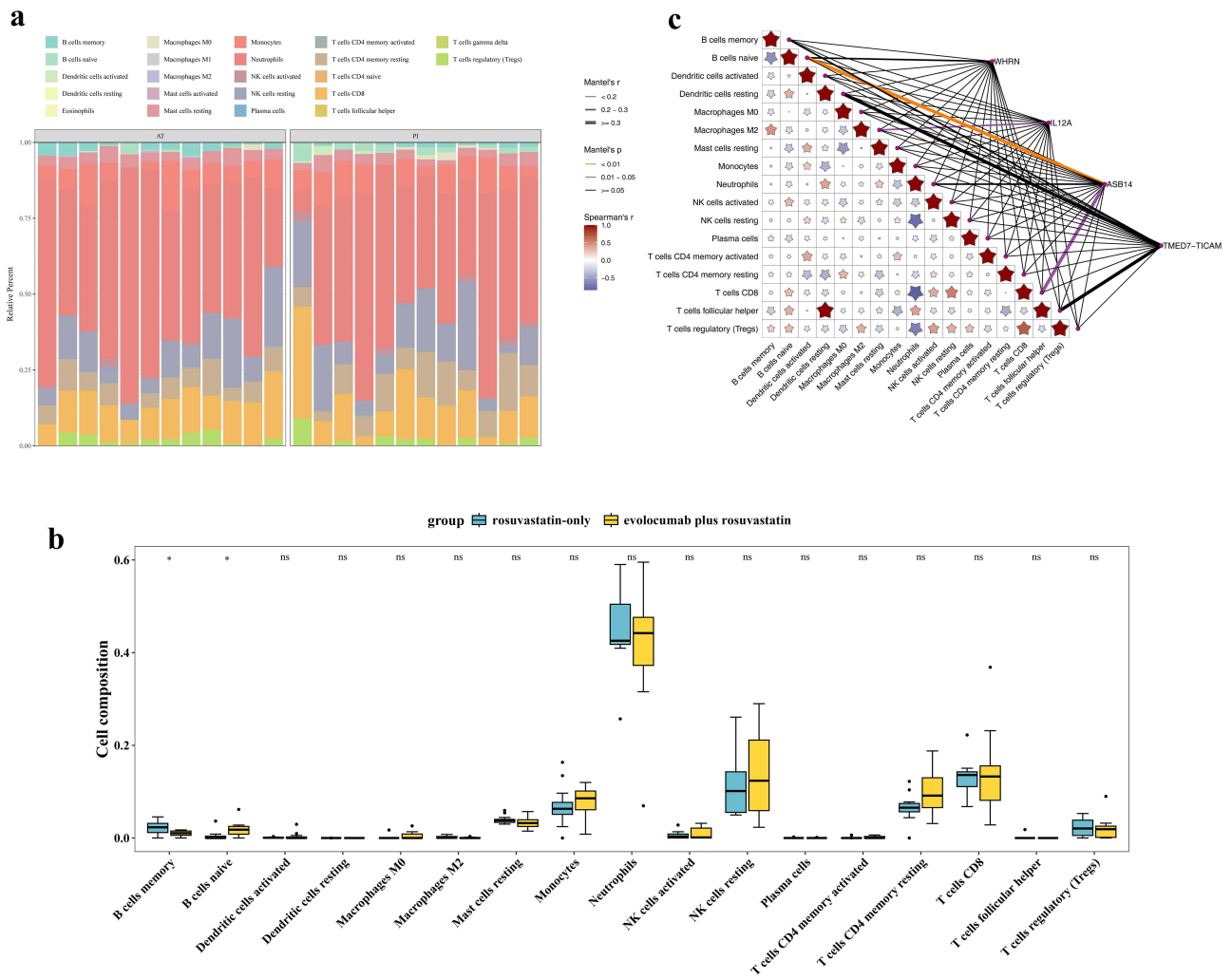

Figure 4 Immune infiltration analysis and biomarker-immune cell correlation. (**a**) Heatmap showing relative proportions of different immune cell types. (**b**) Violin plots of immune cell composition displaying various immune cell types. (**c**) Correlation heatmap between biomarkers and immune cells. Mantel's p values, and Spearman correlation coefficients. Mantel's r values < 0.2, 0.2–0.3, ≥ 0.3 represent different correlation strengths; Mantel's p values < 0.01, 0.01–0.05, ≥ 0.05 represent different significance levels. In the figure panels, significance levels are indicated as follows: *p < 0.05, **p < 0.01, *p < 0.001, and ns (not significant, p ≥ 0.05).

Single-Cell Transcriptomic Atlas Construction

After quality control and standardization, the single-cell dataset GSE121893 retained 1,630 high-quality cells (Figure S1a–c). UMAP dimensionality reduction divided cells into 8 distinct clusters (clusters 0–7) (Figure 5a), with clustering tree analysis showing stability across different resolution parameters. Resolution 0.9 was selected for subsequent analysis to ensure proper cell population separation (Figure 5b). After normalization, 2,000 highly variable genes were identified (Figure S1d). PCA optimization revealed that the first 16 principal components contained major biological variation (Figure S1e), with JackStraw testing confirming statistical significance of the first 5 components ($p < 0.05$) (Figure S1f).

Based on known marker genes, 8 cell clusters were annotated into 5 major cell types: cardiomyocytes (CM), endothelial cells (EC), fibroblasts (FB), macrophages (MP), and smooth muscle cells (SMC) (Figure 5c). Dot plots showed characteristic marker gene expression patterns: cardiomyocytes highly expressed TNNT2, TTN; endothelial cells specifically expressed VWF, CDH5; fibroblasts mainly expressed FN1, VIM; macrophage markers included CD163, CSF1R; smooth muscle cells expressed MYH11, ACTA2 (Figure 5d). UMAP visualization demonstrated clear morphological separation of these cell types in 2D space (Figure 5e), with heatmaps further validating marker gene specificity and annotation accuracy (Figure 5f and g).

https://doi.org/10.2147/IJGM.S603395

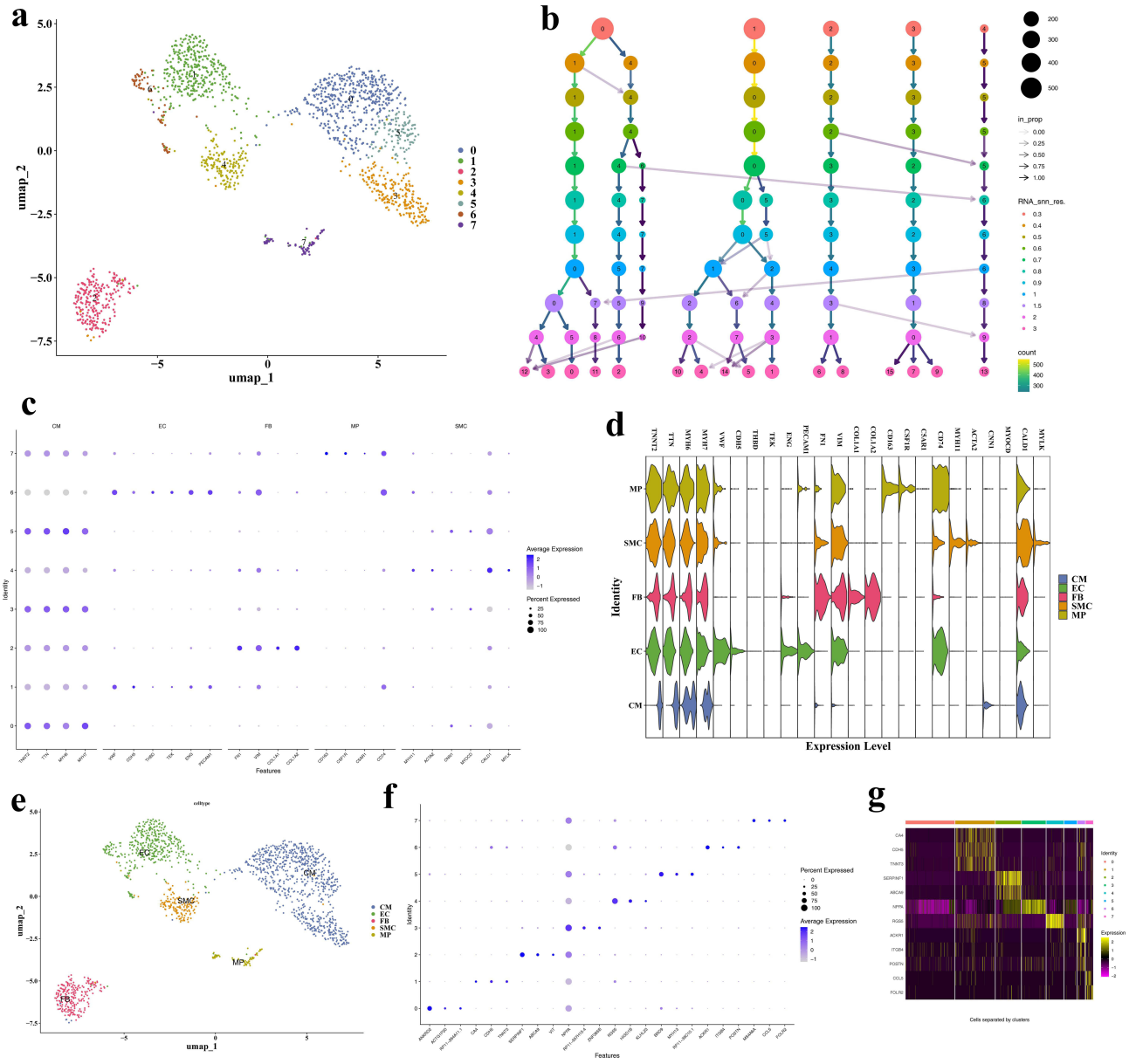

Figure 5 Single-cell RNA sequencing clustering analysis and cell type identification. (**a**) UMAP clustering plot showing the distribution of 8 cell clusters in 2D space with different colors, demonstrating spatial separation characteristics of each cluster. (**b**) Clustering tree plot displaying cluster relationships with different colors or node sizes representing cluster quantities. (**c**) Heatmap of cell type marker gene expression showing average expression levels (0–5 gradient) and expression percentages (25%–100%) of marker genes in cardiomyocytes (CM), endothelial cells (EC), fibroblasts (FB), macrophages (MP), and smooth muscle cells (SMC). Color intensity reflects expression levels to assist cell type annotation. (**d**) UMAP distribution plot of cell types showing the distribution of five cell types (CM, EC, FB, MP, SMC) in 2D space with different colors. (**e**) Cell Type UMAP Distribution Plot: Displaying the distribution of 5 cell types - cardiomyocytes (CM), endothelial cells (EC), fibroblasts (FB), macrophages (MP), and smooth muscle cells (SMC). (**f**) Dot plot of cluster marker genes with dot color representing average expression levels of marker genes in different clusters. Darker colors and larger dots indicate higher expression levels and broader expression ranges. (**g**) Heatmap of top cluster marker genes showing relative expression levels of characteristic marker genes in 8 clusters, with red-blue color gradient representing expression levels (red: high expression, blue: low expression).

Key Cell Identification and Characterization Based on Candidate Biomarker Expression

Cell composition analysis revealed differences in the relative proportions of five major cell types between CAD and control groups, with cardiomyocytes predominating in the CAD group (Figure 6a). UMAP analysis by disease status showed distinct cell type distributions, particularly different spatial distribution patterns of cardiomyocytes (Figure 6b and c).

Expression pattern analysis of key candidate biomarkers showed that *DFNB31 (WHRN alias)* and ASB14 exhibited differential expression across cell types: *DFNB31* was mainly expressed in cardiomyocytes and endothelial cells, while *ASB14* was most prominent in cardiomyocytes (Figure 6d and e). Key cell definition results showed that *ASB14* exhibited

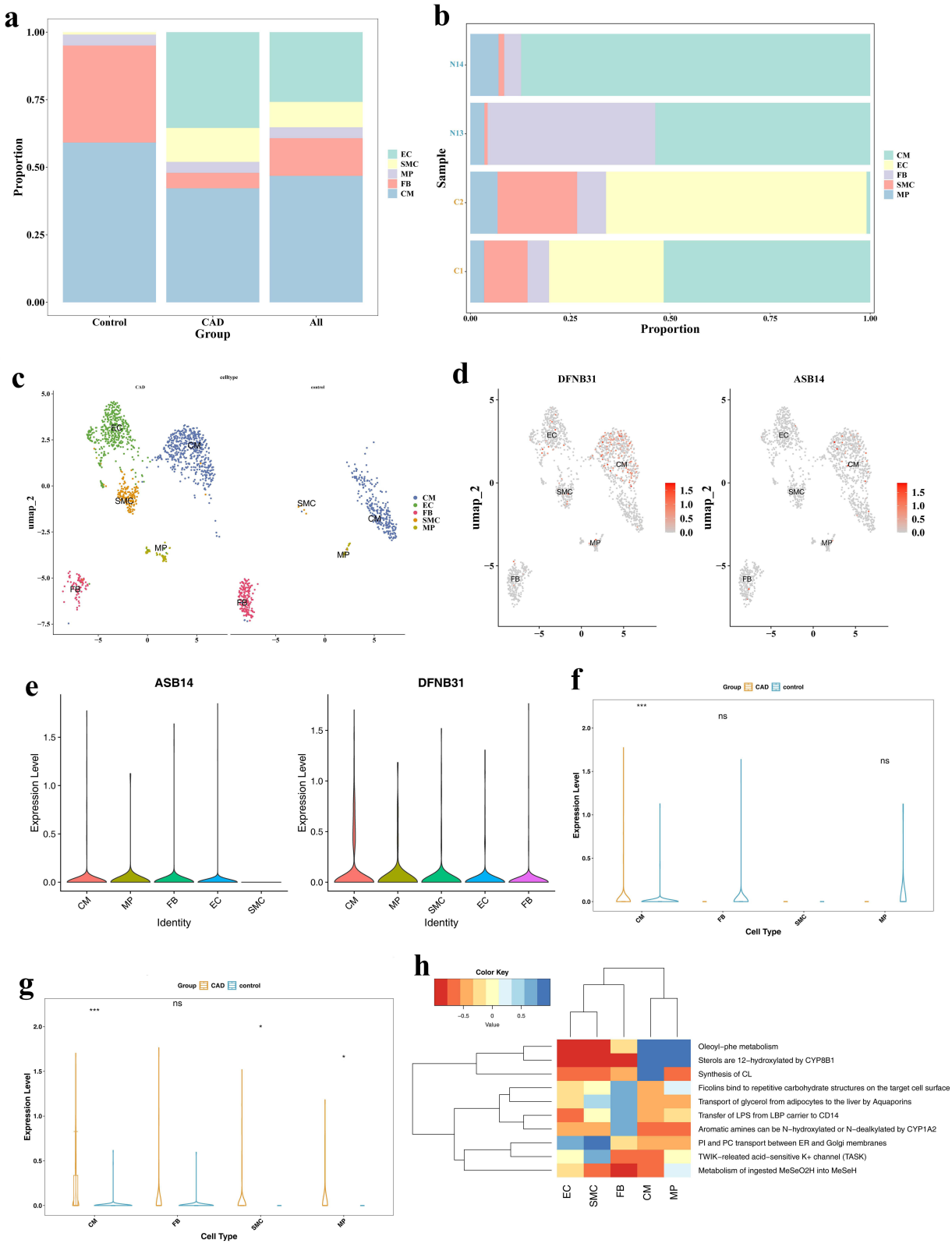

Figure 6 Key cell identification and biomarker expression analysis across cell types. (**a**) Bar plot showing cell proportions across different groups. (**b**) Heatmap of cell proportions in samples. Darker colors represent higher proportions of corresponding cell types in each sample. (**c**) UMAP plot of cell types grouped by disease status. (**d**) UMAP expression plots of biomarkers in cell types. Left panel shows *DFNB31* expression distribution, right panel shows *ASB14* expression distribution. Darker colors indicate higher expression levels. (**e**) Violin plots of biomarker expression in MP and SMC cells. Left panel shows *ASB14* expression levels in MP and SMC, right panel shows *DFNB31* expression levels. (**f**) Bar plot of *ASB14* expression across different cell types. (**g**) Bar plot of *DFNB31* expression across different cell types. (**h**) GSVA enrichment analysis heatmap, with red representing high enrichment and blue representing low enrichment. *** indicate $p < 0.001$, * indicate $p < 0.05$, ns indicate not significant.

https://doi.org/10.2147/IJGM.S603395

extremely significant expression differences in cardiomyocytes ($p < 0.001$) but no significant differences in other cell types (Figure 6f). *DFNB31* showed significant differences in cardiomyocytes, smooth muscle cells, and macrophages, with the most significant difference in cardiomyocytes (Figure 6g). Based on these findings, cardiomyocytes were defined as key cells. Principal component analysis confirmed data quality with significant biological variation captured in the first 9 PCs (Figure S2a and b). Further subtype analysis revealed 3 cardiomyocyte subclusters with distinct functional specializations (Figure S2c–f). Reactome functional enrichment analysis revealed cell type-specific biological functions across metabolic pathways, ion channels, and lipid transport (Figure 6h).

Cell Communication Networks and Pseudotime Trajectory Analysis

CellChat analysis revealed that five cell types (cardiomyocytes, endothelial cells, fibroblasts, smooth muscle cells, macrophages) in the CAD group formed complex communication networks, with strong signaling between cardiomyocytes and fibroblasts and important endothelial cell connections (Figure 7a and b). The control group showed simplified networks involving only four cell types with reduced endothelial cell activity (Figure 7c and d).

Sender-receiver analysis demonstrated that fibroblasts served as primary signal senders in CAD, while cardiomyocytes functioned as both senders and receivers (Figure 7e and f). Ligand-receptor analysis revealed enriched signaling mechanisms in CAD, including collagen-related matrix signals, growth factor pathways, adhesion molecules, and inflammatory signals (APP-CD74), with PTN-NCL showing the highest communication probability from fibroblasts to cardiomyocytes (Figure 7g and h).

Pseudotime analysis revealed cardiomyocyte differentiation trajectories with distinct disease-related patterns (Figure 8a–d). Disease-stratified analysis showed CAD group cells predominantly distributed in states 1, 6, and 7, while control group cells were mainly in states 4 and 5, indicating pathological differentiation (Figure 8e).

Expression analysis revealed that both *ASB14* and *DFNB31* maintained differential expression between groups throughout pseudotime (Figure 8f) and exhibited "inverted U-shaped" expression patterns, with *ASB14* peaking early and *DFNB31* peaking mid-trajectory (Figure 8g–i). Branch enrichment analysis demonstrated functional specialization: branch C1 enriched apoptosis regulation genes, branch C3 involved mitochondrial function (acetyl-CoA biosynthesis, respirasome assembly), while other branches related to immune response and cell migration, indicating cardiomyocyte differentiation reprogramming in CAD (Figure 8j).

Discussion

There is a close connection between BHS and CHD, and the inflammatory response plays an important role in the progression of both diseases. Therefore, inflammation management and comprehensive interventions are crucial for improving the prognosis of these patients. Evolocumab significantly reduces the risk of cardiovascular and cerebrovascular events in patients with CHD and acute ischemic stroke by significantly lowering the LDL-C level.[35,36] However, the targets and mechanisms of the inflammatory effects of Evolocumab in BHS patients with CHD history are not yet clear. Therefore, in this study, by implementing quality control, differential analysis, GO and KEGG enrichment analysis, construction of the PPI network, and machine learning techniques, we successfully identified four crucial gene expressions (*WHRN, IL12A, ASB14, TMED7-TICAM2*) that are regulated by evolocumab in patients with BHS who also have CHD history. Subsequently, we delved deeper into these key genes' functions and regulatory mechanisms through GeneMANIA, immune infiltration, and molecular regulatory network analysis. Since this study is observational and transcriptomic in nature, all interpretations regarding molecular mechanisms should be regarded as hypothesis-generating, and no causal inferences can be drawn from the current data.

Ankyrin repeats and suppressor of cytokine signaling box 14 (ASB14) are members of the suppressor of cytokine signaling (SOCS) box family. Structurally, it comprises an ankyrin repeat domain and a SOCS box domain. It is pivotal in the cardiovascular system, predominantly associated with the negative regulation of cytokine signal transduction.[37] Existing studies have demonstrated that ASB14 directly inhibits the activity of Janus kinase (JAK) tyrosine kinase via the kinase inhibitory region (KIP) and suppresses the Toll-like receptor (TLR) - nuclear factor kappa B (NF-κB) pathway,[38,39] and regulates the expression of inflammatory factors influences the magnitude of the inflammatory

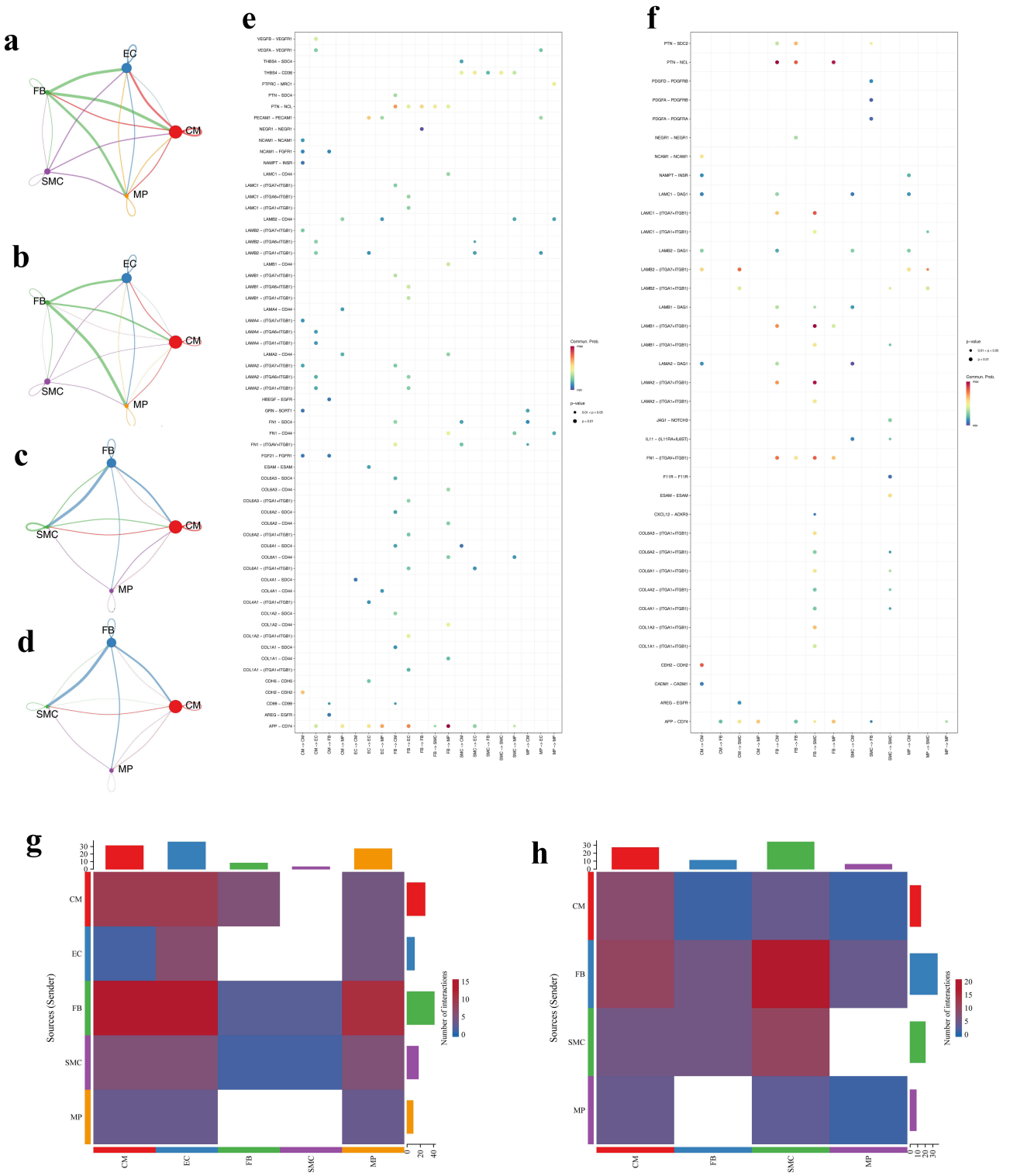

Figure 7 Cell-cell communication network analysis between CAD and control groups. (**a**) Number of intercellular interactions in CAD group. (**b**) Intercellular interaction weight/strength in the CAD group. (**c**) Number of intercellular interactions in the control group. (**d**) Intercellular interaction weight/strength in control group. (**e**) Bubble plot of ligand-receptor interactions between cells in the CAD group. Bubble size represents communication probability, and colors distinguish p-value ranges ($0.01 < p < 0.05$ and $p < 0.01$), with darker colors indicating higher significance. (**f**) Bubble plot of ligand-receptor interactions between cells in the control group. Bubble size reflects communication probability, and colors distinguish p-value ranges ($0.01 < p < 0.05$ and $p < 0.01$), showing various ligand-receptor pairs (such as PTN-NCL, COL1A1-(ITGA1 +ITGB1), etc.) interactions between different cell types, intuitively presenting the molecular mechanism characteristics of cellular communication in the control group. (**g**) Number of interactions with cells as senders in CAD group. Left panel distinguishes CM and EC sender cell types with different colors, showing their interaction numbers with other cells; right panel distinguishes FB, SMC, MP, EC as four sender cell types with colors, presenting their interaction numbers. (**h**) Number of interactions with cells as senders in control group. Left panel distinguishes CM and FB sender cell types with colors, showing their interaction numbers; the right panel distinguishes SMC, MP, CM, FB as four sender cell types with colors, presenting their interaction numbers.

https://doi.org/10.2147/IJGM.S603395

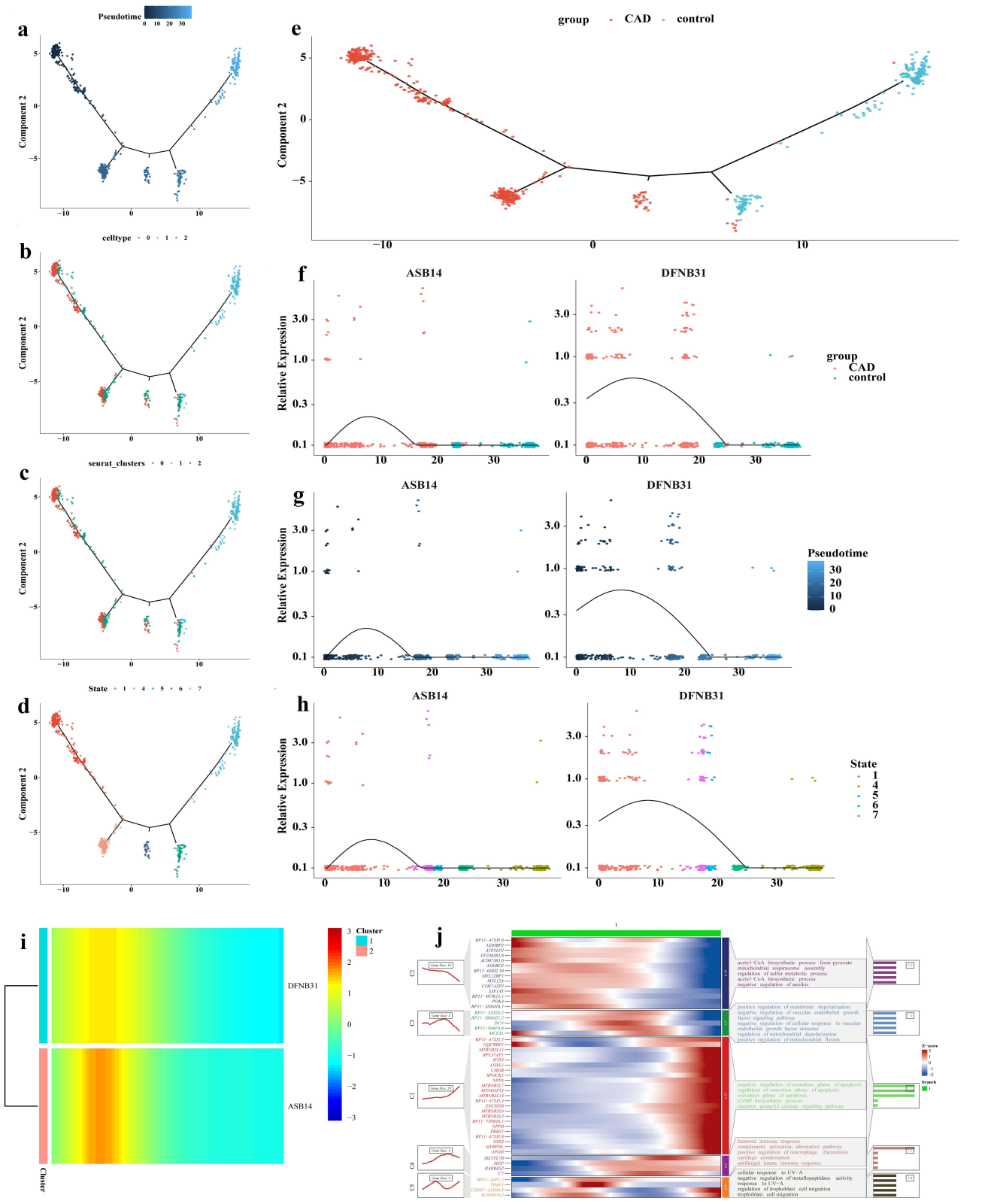

Figure 8 Pseudotime trajectory analysis of cardiomyocytes and gene expression dynamics. (**a**) Pseudotime trajectory plot of cardiomyocytes (CM) with color gradient representing pseudotime. (**b**) Cardiomyocyte trajectory plot grouped by cell type. (**c**) Cardiomyocyte trajectory plot grouped by Seurat clustering. (**d**) Cardiomyocyte trajectory plot grouped by state. (**e**) Cardiomyocyte trajectory plot grouped by disease status. (**f**) Heatmap of key gene expression in cardiomyocytes across different groups, with color gradient reflecting expression levels - darker colors indicate higher expression. (**g**) Heatmap of key gene expression in cardiomyocytes during pseudotime progression, with a color gradient intuitively showing gene expression changes over time. (**h**) Heatmap of key gene expression in cardiomyocytes across different states, with color differences reflecting gene expression characteristics under different differentiation states. (**i**) Heatmap of key gene expression in pseudotime clusters, with red representing high expression and blue representing low expression. (**j**) Enrichment analysis plot of cardiomyocyte differentiation branches.

https://doi.org/10.2147/IJGM.S603395

response. Additionally, high expression of *ASB14* can activate the activity of E3 ubiquitination ligase, initiate protein ubiquitination, and facilitate the clearance of variant proteins.[40]

In the immune cell infiltration analysis, the key gene *ASB14* exhibited the negative correlation with natural killer cells. This finding further implies that elevated expression of *ASB14* is associated with a reduction in the release of pro-inflammatory factors. These results propose a potential mechanism: evolocumab treatment may regulate inflammatory pathways by altering the expression pattern of the *ASB14* gene and related immune cell populations. However, it is important to emphasize that these correlations derived from immune infiltration should be regarded as hypothesis-generating observations rather than definitive causal relationships. The specific mechanisms underlying the associations between *ASB14* expression, natural killer (NK) cell function, and inflammatory outcomes still need to be verified through controlled experimental studies to establish causal relationships.

TMED7 and *TICAM2* (Transmembrane emp24 domain-containing protein 7 and Toll interleukin 1 receptor (TIR) domain-containing adaptor molecule 2) are two distinct genes, each situated on chromosome 5. Bioinformatics analyses, corroborated by experimental evidence, have revealed transcriptional readthrough from the *TMED7* gene into the *TICAM2 (TRAM)* gene. This phenomenon gives rise to the expression of three proteins: TMED7, TRAM, and TAG, as documented in previous studies.[41,42] These proteins are detectable across various tissues, albeit with varying abundance levels.[43]

TMED7, a 224-amino acid protein, harbors the gold domain of TAG but lacks the TIR domain. As a member of the p24 transmembrane protein γ family, TMED7 is primarily involved in endoplasmic reticulum-Golgi vesicle trafficking and regulating transmembrane protein stability. Notably, it plays a pivotal role in Toll-like receptor 4 (TLR4) signal transduction.[43,44] The gold domain of TMED7 proteins confers their involvement in vesicle transport processes. Recent investigations have elucidated that TMED7 is an essential structural protein for forming a stable complex between TLR4 and its extracellular domain during the protein's translocation from the endoplasmic reticulum to the cell surface via the Golgi apparatus. TLR4, in turn, initiates the activation of downstream intracellular pathways, such as the NF-κB pathway.[45,46]

TICAM2, or TRAM, is a crucial adaptor protein for endosomal TLR4-mediated signal transduction. Through its TIR domain, TICAM2 interacts with TLR4 and TICAM1,[47] participating in the TLR4-mediated MyD88-independent signaling pathway and regulating the release of inflammatory factors. The endosomal TLR4-TICAM2-TICAM1 complex can induce type I interferon production.[48] However, overactivation of this complex exacerbates inflammatory injury, promoting the expression of proinflammatory cytokines, including IL-6 and TNF-α, via its downstream RIP1-TRAF6-NF-κB axis.[49] Additionally, some studies have suggested that TICAM2 may contribute to the systemic inflammatory response by facilitating neutrophil depletion.[50] The TLR4/NF-κB signaling pathway is a central player in the inflammatory response. Excessive activation of TLR4 triggers the production of many inflammatory factors intricately associated with the pathogenesis and progression of cardiovascular diseases.[51]

Given their roles, TICAM2, a key adaptor protein in the TLR4-mediated immune response and inflammatory activation pathway, and TMED7, a regulatory transport protein of the signaling pathway, may exhibit a synergistic effect during the inflammatory response. This synergy potentially indirectly impacts the release of inflammatory factors by modulating TLR4 function. In the present study, gene detection of peripheral blood samples from patients with BHS with CHD history demonstrated that the expression of the *TMED7-TICAM2* gene was significantly downregulated in the treatment group administered evolocumab. However, this finding based on bulk RNA-seq data can only serve as hypothesis-generating evidence. This study speculates that evolocumab treatment may be associated with altered expression of the *TMED7-TICAM2* gene through some as-yet-unclear mechanism, but its specific molecular mechanism, whether it directly affects the localization and functional activity of TLR4, and its exact association with inflammatory responses still need to be confirmed through further functional verification experiments. These findings provide valuable candidate targets for future mechanistic research.

Analysis of immune cell infiltration in this study revealed a strong positive correlation between TMED7-TICAM2 and activated/resting NK cells. Based on this correlation finding, we speculate that the changes in TMED7-TICAM2 expression may be related to the activity status of peripheral blood immune cells. Although the KEGG pathway enrichment analysis of TMED7-TICAM2 did not identify direct inflammatory regulatory pathways, the enriched oxidative phosphorylation pathway suggests a potential mechanistic hypothesis: the reactive oxygen species (ROS) generated in this process may act as second messengers to participate in the activation of the NF-κB signaling pathway, thereby affecting the release of inflammatory factors. It should be emphasized that these results of correlation analysis based on immune infiltration should be regarded as

hypothesis-generating findings rather than conclusive evidence of causal relationships. We speculate that evolocumab treatment may indirectly affect the functional status of immune cells by regulating the expression patterns of candidate biomarkers such as TMED7-TICAM2. However, these speculations need to be confirmed through further mechanistic studies and experimental verification to clarify the specific causal relationships and molecular mechanisms.

The *IL12A* gene encodes the p35 subunit of interleukin 12 (IL-12), which, in conjunction with the p40 subunit encoded by the *IL12B* gene, forms a functional IL-12 heterodimer. IL-12 is predominantly secreted by activated antigen-presenting cells, including dendritic cells, macrophages, and B cells.[52] Upon binding to the IL-12 receptor, it activates the JAK-STAT signaling pathway. This activation drives the differentiation of naïve CD4+ T cells into the Th1 phenotype and enhances the cytotoxicity of NK cells and T cells, thereby augmenting the cellular immune response.[53]

Beyond its well-established roles in anti-infection and anti-tumor immunity, emerging evidence in recent years has highlighted the critical involvement of IL-12 in the pathogenesis of cardiovascular and cerebrovascular diseases, such as atherosclerosis, myocardial infarction, and ischemic stroke. Multiple lines of evidence support the role of IL-12 in atherosclerotic lesions. Clinicopathological studies have demonstrated the enrichment of IL-12 in human atherosclerotic plaques, where it accelerates plaque progression by triggering local inflammatory responses.[54] Additionally, circulating IL-12 levels have emerged as a potential biomarker associated with cardiovascular risk. A cross-sectional study confirmed a significant positive correlation between IL-12 levels and arterial stiffness, as measured by pulse wave velocity.[54] In patients with acute coronary syndrome, elevated plasma IL-12 levels have been shown to have independent prognostic value for patients with ST-segment elevation myocardial infarction.[55] In ischemic stroke patients, studies have indicated that serum IL-12 levels during the acute phase are positively correlated with the volume of brain injury and the degree of neurological deficit, suggesting its participation in the post-ischemic inflammatory cascade.[56] Collectively, these findings suggest that IL-12 may play a pivotal role in the pathophysiology of atherosclerotic cardiovascular and cerebrovascular diseases.

Preclinical investigations have further elucidated the pro-atherosclerotic mechanisms of IL-12. Gene-edited animal models have shown that IL-12 deficiency, exemplified by IL-12 p40−/− apoE−/− mice, significantly reduces macrophage infiltration and plaque area in the aortic root induced by a high-fat diet.[57] Intervention studies have demonstrated that vaccination with an IL-12 vaccine in LDLR−/− mice leads to increased collagen deposition in plaques and decreased serum interferon-γ levels, indicating that immune modulation can inhibit lesion progression.[58] Moreover, treatment with recombinant IL-12 in ApoE−/− mice accelerates atherosclerosis, characterized by increased CD3+ T cell infiltration in plaques and an enlarged lesion area.[59] These findings collectively support the pro-atherosclerotic effect of IL-12 and underscore its potential as a therapeutic target.

This study revealed a significant upregulation of *IL12A* gene expression in BHS with CHD history patients who were treated with evolocumab. However, the p35 subunit encoded by IL12A requires association with the p40 subunit to form a heterodimer with biological activity. Therefore, further investigation of p40 subunit expression and the biological activity of IL-12 is warranted to determine whether evolocumab indeed upregulates IL-12 expression. Additionally, IL-12 has a relatively large molecular weight (approximately 70 kDa), resulting in significantly limited efficiency in crossing the blood-brain barrier compared to low-molecular-weight pro-inflammatory factors (eg., IL-6, 21 kDa), thereby mitigating its potential neuroinflammatory injury. Future studies should focus on further verifying the regulatory effect of evolocumab on IL-12 through dynamic monitoring of blood-brain barrier permeability, quantitative analysis of IL-12 in cerebrospinal fluid, and the use of neuroinflammation animal models.

The *WHRN* gene encodes the whirlin protein, a scaffold protein containing PDZ domains.[60] PDZ domains are known to mediate protein–protein interactions involved in mechanosensation, cytoskeletal anchorage, and the assembly of signaling complexes.[61] In cardiomyocytes, the non-sarcomeric cytoskeleton acts as a bridge connecting sarcomeres, the cell membrane, and the extracellular matrix, and is essential for cardiac contractile function and mechanotransduction.[62,63]

In the present study, *WHRN* expression was significantly upregulated in the evolocumab combined with rosuvastatin group. Although this observation suggests that *WHRN* may be involved in cytoskeletal organization or mechanotransduction pathways under evolocumab treatment, direct experimental evidence remains lacking. Given the limited literature regarding the role of *WHRN* in cardiovascular and immune contexts, this finding should be regarded as hypothesis-generating and requires further functional validation in future studies.

Our single-cell analysis identified cardiomyocytes as key cells, which holds significant biological importance. Cardiomyocytes are critical participants in the pathophysiological process of cerebrocardiac syndrome. Cerebrovascular events can directly affect the structure and function of cardiomyocytes through the neuro-cardiac axis. The surge in catecholamines caused by brain injury can lead to cardiomyocyte necrosis, hypertrophy, and fibrosis,[64] and catecholamines directly released by sympathetic nerve endings have a direct toxic effect on adjacent cardiomyocytes.[1] At the molecular level, this process involves mechanisms such as *FOXO* gene activation, regulation of protein degradation, and metabolic reprogramming of cardiomyocytes.[65] The four candidate biomarkers (*WHRN, IL12A, ASB14, TMED7-TICAM2*) showed the most significant and consistent CAD-related expression changes in cardiomyocytes, providing cell-type-specific validation for the candidate biomarkers we identified from bulk RNA-seq. Of particular note is the highly specific expression of *ASB14* in cardiomyocytes. Pseudotime analysis revealed that cardiomyocytes in the CAD group were mainly distributed in pathological differentiation states (State 1, 6, 7), while the control group remained in relatively healthy differentiation states (State 4, 5), suggesting that evolocumab treatment may exert a protective effect by regulating the differentiation trajectory of cardiomyocytes. The results of single-cell analysis further verify the reliability of candidate biomarkers and provide a basis for the development of cardiomyocyte-specific therapeutic targets and diagnostic tools for precision medicine.

There are limited studies investigating transcriptomic alterations associated with PCSK9 inhibitor therapy in patients with cardiovascular diseases. The FOURIER trial has demonstrated that evolocumab significantly reduces cardiovascular events.[12,66] However, no independent transcriptomic substudies from this trial have been publicly reported. Our findings complement these previous observations, suggesting that evolocumab may be associated with expression changes in genes involved in immune regulation (*IL12A*), protein ubiquitination (*ASB14*), and TLR4 signal transduction (*TMED7-TICAM2*). Nevertheless, direct comparisons with prior work are constrained, as most earlier transcriptomic analyses were performed in preclinical models or distinct patient populations. Further investigations in larger independent cohorts are warranted to verify the reproducibility of the transcriptomic signatures identified in the present study.

This study provides transcriptomic insights into exploring potential gene expression changes in patients with BHS who have a history of CHD following evolocumab treatment. Through differential gene expression analysis and pathway enrichment methods, we identified several candidate biomarkers (*WHRN, IL12A, ASB14, and TMED7-TICAM2*) that may be associated with the therapeutic effects of evolocumab. However, these findings require extensive validation and should not be regarded as definitive mechanistic conclusions. Several important limitations must be acknowledged. First, it was designed as a preliminary exploratory analysis with a small sample size (n=24), and no formal statistical power calculation was performed, raising potential overfitting concerns. Confounding factors including rosuvastatin dosage, baseline LDL-C levels and stroke severity were not incorporated into the multivariate model, which may limit the generalizability of the present findings. Second, only acute-phase blood samples were collected without longitudinal transcriptomic profiling; thus, the duration and persistence of evolocumab-induced transcriptomic alterations remain undetermined. Moreover, the non-standardized timing of treatment initiation might have interfered with gene expression patterns. Third, the external validation dataset GSE113079 enrolled coronary artery disease patients rather than BHS individuals. Despite shared pathophysiological features and a history of coronary heart disease among BHS patients, this cohort mismatch may compromise the robustness of the validation results. Additionally, several biomarkers yielded AUC values below 0.7 in the external dataset, implying modest diagnostic efficacy and necessitating cautious interpretation of these results.

Fourth, statistical significance does not equate to genuine biological relevance. Although differential gene expression, AUC performance and immune cell differences reached statistical significance, the small effect sizes, limited sample size and lack of orthogonal validation suggest that these outcomes should be considered hypothesis-generating rather than conclusive. The lack of enriched terms in GO biological process and molecular function categories does not rule out biological implications, as the enriched cellular component terms (granules and lysosomes) are functionally linked to inflammation. Meanwhile, the limited number of significantly altered immune cell subtypes indicates that the immunomodulatory effects of evolocumab may be restricted to specific subpopulations rather than exerting broad-spectrum activity.

Future large-scale retrospective studies with clinical endpoints are required to reduce inherent bias, and further validation of these key genes should be conducted using molecular experiments and animal models.

Conclusion

This pilot study provides preliminary insights into the molecular mechanisms of evolocumab in treating Brain-Heart Syndrome with a coronary heart disease history, identifying four inflammation-related biomarkers. These findings suggest potential targets for future investigation; however, given the exploratory nature and small sample size, further experimental and clinical validation is required before any therapeutic application.

Data Sharing Statement

The datasets generated during and/or analysed during the current study are available from the corresponding author on reasonable request. The raw sequence data reported in this paper have been deposited in the Genome Sequence Archive (Genomics, Proteomics & Bioinformatics 2025) in National Genomics Data Center (Nucleic Acids Res 2025), China National Center for Bioinformation/Beijing Institute of Genomics, Chinese Academy of Sciences (GSA-Human: HRA014845) that are publicly accessible at https://ngdc.cncb.ac.cn/gsa-human. Data requests may be directed to the corresponding author Xiaofei Ji.

Ethics Approval

This study was performed in line with the principles of the Declaration of Helsinki. The study was approved by the Ethics Committee of the First Affiliated Hospital of Dalian Medical University (Approval number: PJ-KS-KY-2025-958).

Acknowledgments

We would like to express our heartfelt gratitude to the participants and their guardians for their cooperation.

Funding

This research received no specific grant from any funding agency in the public, commercial, or not-for-profit sectors and was self-funded by the researchers.

Disclosure

The authors have no relevant financial or non-financial interests to disclose for this work.

References

1. Chen Z, Venkat P, Seyfried D. et al. Brain-Heart Interaction: cardiac Complications After Stroke. *Circ Res*. 2017;121(4):451–468. doi:10.1161/CIRCRESAHA.117.311170
2. Tang H, Xing X, Han Y, et al. A Retrospective Study of Brain-Heart Syndrome in Patients with Acute Cerebrovascular Diseases. *Risk Manag Healthc Policy*. 2024;17:2161–2168. doi:10.2147/RMHP.S467205
3. Gao S, Liu J. Association between circulating oxidized low-density lipoprotein and atherosclerotic cardiovascular disease. *Chronic Dis Transl Med*. 2017;3(2):89–94. doi:10.1016/j.cdtm.2017.02.008
4. Kong Q, Ma X, Wang C, et al. Patients with Acute Ischemic Cerebrovascular Disease with Coronary Artery Stenosis Have More Diffused Cervicocephalic Atherosclerosis. *J Atheroscler Thromb*. 2019;26(9):792–804. doi:10.5551/jat.47464
5. Bianchi ME. DAMPs, PAMPs and alarmins: all we need to know about danger. *J Leukoc Biol*. 2007;81(1):1–5. doi:10.1189/jlb.0306164
6. Kawai T, Akira S. The role of pattern-recognition receptors in innate immunity: update on Toll-like receptors. *Nat Immunol*. 2010;11(5):373–384. doi:10.1038/ni.1863
7. Bekkering S, Quintin J, Joosten LA, et al. Oxidized low-density lipoprotein induces long-term proinflammatory cytokine production and foam cell formation via epigenetic reprogramming of monocytes. *Arterioscler Thromb Vasc Biol*. 2014;34(8):1731–1738. doi:10.1161/ATVBAHA.114.303887
8. van der Valk FM, Bekkering S, Kroon J, et al. Oxidized Phospholipids on Lipoprotein(a) Elicit Arterial Wall Inflammation and an Inflammatory Monocyte Response in Humans. *Circulation*. 2016;134(8):611–624. doi:10.1161/CIRCULATIONAHA.116.020838
9. Shapiro MD, Fazio S. PCSK9 and Atherosclerosis - Lipids and Beyond. *J Atheroscler Thromb*. 2017;24(5):462–472. doi:10.5551/jat.RV17003
10. Petersen-Uribe Á, Kremser M, Rohlfing AK, et al. Platelet-Derived PCSK9 Is Associated with LDL Metabolism and Modulates Atherothrombotic Mechanisms in Coronary Artery Disease. *Int J Mol Sci*. 2021;22(20):11179. doi:10.3390/ijms222011179
11. Tang ZH, Peng J, Ren Z, et al. New role of PCSK9 in atherosclerotic inflammation promotion involving the TLR4/NF-κB pathway. *Atherosclerosis*. 2017;262:113–122. doi:10.1016/j.atherosclerosis.2017.04.023

12. Sabatine MS, Giugliano RP, Keech AC, et al. Evolocumab and Clinical Outcomes in Patients with Cardiovascular Disease. *N Engl J Med*. 2017;376 (18):1713–1722. doi:10.1056/NEJMoa1615664
13. Apaijai N, Moisescu DM, Palee S, et al. Pretreatment With PCSK9 Inhibitor Protects the Brain Against Cardiac Ischemia/Reperfusion Injury Through a Reduction of Neuronal Inflammation and Amyloid Beta Aggregation. *J Am Heart Assoc*. 2019;8:e010838.
14. Kanani J, Sheikh MI. Exploring Nontraumatic Brain Hemorrhage in Sudden and Unexpected Deaths: a Novel Autopsy-Based Investigation. *Asian J Neurosurg*. 2025;20(1):126–131. doi:10.1055/s-0044-1800811
15. Tian W, Cao H, Li X, et al. Adjunctive PCSK9 Inhibitor Evolocumab in the Prevention of Early Neurological Deterioration in Non-cardiogenic Acute Ischemic Stroke: a Multicenter, Prospective, Randomized, Open-Label, Clinical Trial. *CNS Drugs*. 2025;39(2):197–208. doi:10.1007/s40263-024-01145-5
16. Momtazi-Borojeni AA, Sabouri-Rad S, Gotto AM, et al. PCSK9 and inflammation: a review of experimental and clinical evidence. *Eur Heart J Cardiovasc Pharmacother*. 2019;5(4):237–245. doi:10.1093/ehjcvp/pvz022
17. Aguiar JA, Tamminga A, Lobb B, et al. The impact of cigarette smoke exposure, COPD, or asthma status on ABC transporter gene expression in human airway epithelial cells. *Sci Rep*. 2019;9(1):153. doi:10.1038/s41598-018-36248-9
18. Love MI, Huber W, Anders S. Moderated estimation of fold change and dispersion for RNA-seq data with DESeq2. *Genome Biol*. 2014;15(12):550. doi:10.1186/s13059-014-0550-8
19. Gu Z, Hübschmann D. Make Interactive Complex Heatmaps in R. *Bioinformatics*. 2022;38:1460–1462. doi:10.1093/bioinformatics/btab806
20. Wu T, Hu E, Xu S, et al. clusterProfiler 4.0: a universal enrichment tool for interpreting omics data. *Innovation*. 2021;2(3):100141. doi:10.1016/j.xinn.2021.100141
21. Xiong W, Zhong J, Li Y, et al. Identification of Pathologic Grading-Related Genes Associated with Kidney Renal Clear Cell Carcinoma. *J Immunol Res*. 2022;2022:2818777. doi:10.1155/2022/2818777
22. Smoot ME, Ono K, Ruscheinski J, et al. Cytoscape 2.8: new features for data integration and network visualization. *Bioinformatics*. 2011;27 (3):431–432. doi:10.1093/bioinformatics/btq675
23. Friedman J, Hastie T, Tibshirani R. Regularization Paths for Generalized Linear Models via Coordinate Descent. *J Stat Softw*. 2010;33(1):1–22. doi:10.18637/jss.v033.i01
24. Kebede MM, Le Cornet C, Fortner RT. In-depth evaluation of machine learning methods for semi-automating article screening in a systematic review of mechanistic literature. *Res Synth Methods*. 2023;14(2):156–172. doi:10.1002/jrsm.1589
25. Yue S, Li S, Huang X, et al. Machine learning for the prediction of acute kidney injury in patients with sepsis. *J Transl Med*. 2022;20(1):215. doi:10.1186/s12967-022-03364-0
26. Gao CH, Chen C, Akyol T, et al. ggVennDiagram: intuitive Venn diagram software extended. *Imeta*. 2024;3(1):e177. doi:10.1002/imt2.177
27. Robin X, Turck N, Hainard A, et al. pROC: an open-source package for R and S+ to analyze and compare ROC curves. *BMC Bioinf*. 2011;12(1):77. doi:10.1186/1471-2105-12-77
28. Zheng J, Zhang T, Guo W, et al. Integrative Analysis of Multi-Omics Identified the Prognostic Biomarkers in Acute Myelogenous Leukemia. *Front Oncol*. 2020;10:591937. doi:10.3389/fonc.2020.591937
29. Zhao Z, Yang H, Ji G, et al. Identification of hub genes for early detection of bone metastasis in breast cancer. *Front Endocrinol (Lausanne)*. 2022;13:1018639. doi:10.3389/fendo.2022.1018639
30. International BR; International BR. Retracted: dysregulated Circulating Apoptosis- and Autophagy-Related lncRNAs as Diagnostic Markers in Coronary Artery Disease. *Biomed Res Int*. 2024;2024:9895849. doi:10.1155/2024/9895849
31. Yu L, Shen N, Shi Y, et al. Characterization of cancer-related fibroblasts (CAF) in hepatocellular carcinoma and construction of CAF-based risk signature based on single-cell RNA-seq and bulk RNA-seq data. *Front Immunol*. 2022;13:1009789. doi:10.3389/fimmu.2022.1009789
32. Wang L, Yu P, Zhou B, et al. Single-cell reconstruction of the adult human heart during heart failure and recovery reveals the cellular landscape underlying cardiac function. *Nat Cell Biol*. 2020;22(1):108–119. doi:10.1038/s41556-019-0446-7
33. Griss J, Viteri G, Sidiropoulos K, et al. ReactomeGSA - Efficient Multi-Omics Comparative Pathway Analysis. *Mol Cell Proteomics*. 2020;19 (12):2115–2125. doi:10.1074/mcp.TIR120.002155
34. Qiu X, Mao Q, Tang Y, et al. Reversed graph embedding resolves complex single-cell trajectories. *Nat Methods*. 2017;14(10):979–982. doi:10.1038/nmeth.4402
35. Mikhail N. Effects of Evolocumab on Cardiovascular Events. *Curr Cardiol Rev*. 2017;13(4):319–324. doi:10.2174/1573403X13666170918165713
36. Kim J, Hong U, Yoon CW, et al. PCSK9 inhibitor in acute ischemic stroke patient receiving mechanical thrombectomy: early outcomes and safety. *Front Neurol*. 2024;15:1375609. doi:10.3389/fneur.2024.1375609
37. Kile BT, Schulman BA, Alexander WS, et al. The SOCS box: a tale of destruction and degradation. *Trends Biochem Sci*. 2002;27(5):235–241. doi:10.1016/S0968-0004(02)02085-6
38. Yoshimura A, Naka T, Kubo M. SOCS proteins, cytokine signalling and immune regulation. *Nat Rev Immunol*. 2007;7(6):454–465. doi:10.1038/nri2093
39. Kanno H, Matsumoto S, Yoshizumi T, et al. Role of SOCS and VHL Proteins in Neuronal Differentiation and Development. *Int J Mol Sci*. 2023;25 (1):24. doi:10.3390/ijms25010024
40. Yang Y, Ma D, Liu B, et al. E3Ubiquitin Ligase ASB14 Inhibits Cardiomyocyte Proliferation by Regulating MAPRE2 Ubiquitination. *Cell Biochem Biophys*. 2024;82(2):715–727. doi:10.1007/s12013-024-01223-x
41. Palsson-McDermott EM, Doyle SL, McGettrick AF, et al. TAG, a splice variant of the adaptor TRAM, negatively regulates the adaptor MyD88-independent TLR4 pathway. *Nat Immunol*. 2009;10(6):579–586. doi:10.1038/ni.1727
42. Prakash T, Sharma VK, Adati N, et al. Expression of conjoined genes: another mechanism for gene regulation in eukaryotes. *PLoS One*. 2010;5 (10):e13284. doi:10.1371/journal.pone.0013284
43. Doyle SL, Husebye H, Connolly DJ, et al. The GOLD domain-containing protein TMED7 inhibits TLR4 signalling from the endosome upon LPS stimulation. *Nat Commun*. 2012;3(1):707. doi:10.1038/ncomms1706
44. Aber R, Chan W, Mugisha S, et al. Transmembrane emp24 domain proteins in development and disease. *Genet Res*. 2019;101:e14. doi:10.1017/S0016672319000090
45. Vatakuti S, Pennings JL, Gore E, et al. Classification of Cholestatic and Necrotic Hepatotoxicants Using Transcriptomics on Human Precision-Cut Liver Slices. *Chem Res Toxicol*. 2016;29(3):342–351. doi:10.1021/acs.chemrestox.5b00491

46. Muñiz M, Nuoffer C, Hauri HP, et al. The Emp24 complex recruits a specific cargo molecule into endoplasmic reticulum-derived vesicles. *J Cell Biol*. 2000;148(5):925–930. doi:10.1083/jcb.148.5.925
47. Funami K, Matsumoto M, Oshiumi H, et al. Functional interfaces between TICAM-2/TRAM and TICAM-1/TRIF in TLR4 signaling. *Biochem Soc Trans*. 2017;45(4):929–935. doi:10.1042/BST20160259
48. Oshiumi H, Sasai M, Shida K, et al. TIR-containing adapter molecule (TICAM)-2, a bridging adapter recruiting to toll-like receptor 4 TICAM-1 that induces interferon-beta. *J Biol Chem*. 2003;278(50):49751–49762. doi:10.1074/jbc.M305820200
49. Zhang T, Ma C, Zhang Z, et al. NF-κB signaling in inflammation and cancer. *MedComm*. 2021;2(4):618–653. doi:10.1002/mco2.104
50. Lin R, Zhang Y, Pradhan K, et al. TICAM2-related pathway mediates neutrophil exhaustion. *Sci Rep*. 2020;10(1):14397. doi:10.1038/s41598-020-71379-y
51. Zhang Y, Liang X, Bao X, et al. Toll-like receptor 4 (TLR4) inhibitors: current research and prospective. *Eur J Med Chem*. 2022;235:114291. doi:10.1016/j.ejmech.2022.114291
52. Hasegawa H, Mizoguchi I, Chiba Y, et al. Expanding Diversity in Molecular Structures and Functions of the IL-6/IL-12 Heterodimeric Cytokine Family. *Front Immunol*. 2016;7:479. doi:10.3389/fimmu.2016.00479
53. van der Heijden T, Bot I, Kuiper J. The IL-12 cytokine family in cardiovascular diseases. *Cytokine*. 2019;122:154188. doi:10.1016/j.cyto.2017.10.010
54. Yong K, Dogra G, Boudville N, et al. Interleukin-12 is associated with arterial stiffness in healthy individuals. *Am J Hypertens*. 2013;26(2):159–162. doi:10.1093/ajh/hps032
55. Zykov MV, Barbarash OL, Kashtalap VV, et al. Interleukin-12 serum level has prognostic value in patients with ST-segment elevation myocardial infarction. *Heart Lung*. 2016;45(4):336–340. doi:10.1016/j.hrtlng.2016.03.007
56. Zaremba J, Losy J. Interleukin-12 in acute ischemic stroke patients. *Folia Neuropathol*. 2006;44:59–66.
57. Davenport P, Tipping PG. The role of interleukin-4 and interleukin-12 in the progression of atherosclerosis in apolipoprotein E-deficient mice. *Am J Pathol*. 2003;163(3):1117–1125. doi:10.1016/S0002-9440(10)63471-2
58. Hauer AD, Uyttenhove C, de Vos P, et al. Blockade of interleukin-12 function by protein vaccination attenuates atherosclerosis. *Circulation*. 2005;112(7):1054–1062. doi:10.1161/CIRCULATIONAHA.104.533463
59. Lee TS, Yen HC, Pan CC, et al. The role of interleukin 12 in the development of atherosclerosis in ApoE-deficient mice. *Arterioscler Thromb Vasc Biol*. 1999;19:734–742. doi:10.1161/01.ATV.19.3.734
60. Zou J, Zheng T, Ren C, et al. Deletion of PDZD7 disrupts the Usher syndrome type 2 protein complex in cochlear hair cells and causes hearing loss in mice. *Hum Mol Genet*. 2014;23(9):2374–2390. doi:10.1093/hmg/ddt629
61. Hong SG, Ashby JW, Kennelly JP, et al. Mechanosensitive membrane domains regulate calcium entry in arterial endothelial cells to protect against inflammation. *J Clin Invest*. 2024;134:1.
62. Seidler U, Singh AK, Cinar A, et al. The role of the NHERF family of PDZ scaffolding proteins in the regulation of salt and water transport. *Ann N Y Acad Sci*. 2009;1165(1):249–260. doi:10.1111/j.1749-6632.2009.04046.x
63. Grimes KM, Prasad V, McNamara JW. Supporting the heart: functions of the cardiomyocyte's non-sarcomeric cytoskeleton. *J Mol Cell Cardiol*. 2019;131:187–196. doi:10.1016/j.yjmcc.2019.04.002
64. Sposato LA, Hilz MJ, Aspberg S, et al. Post-Stroke Cardiovascular Complications and Neurogenic Cardiac Injury: JACC State-of-the-Art Review. *J Am Coll Cardiol*. 2020;76(23):2768–2785. doi:10.1016/j.jacc.2020.10.009
65. Battaglini D, Robba C, Lopes da Silva A, et al. Brain-heart interaction after acute ischemic stroke. *Crit Care*. 2020;24:163. doi:10.1186/s13054-020-02885-8
66. Rosenson RS, Tate A, Mar P, et al. Inhibition of PCSK9 with evolocumab modulates lipoproteins and monocyte activation in high-risk ASCVD subjects. *Atherosclerosis*. 2024;392:117529. doi:10.1016/j.atherosclerosis.2024.117529